Title:

RNA decay defines the response to transcriptional perturbation in leukaemia

Authors and affiliations:

Izabela Todorovski[1,2], Breon Feran[3,4], Zheng Fan[1,2], Sreeja Gadipally[1], David Yoannidis[1], Isabella Y Kong[3,4], Stefan Bjelosevic[1,2], Magnus Zethoven[1], Edwin D Hawkins[3,4], Kaylene J Simpson[1,2], Gisela Mir Arnau[1,2], Anthony T Papenfuss[1,2,3,4], Ricky W Johnstone[1,2,] †*, Stephin J Vervoort[1,2,3,4]†*

[1]Peter MacCallum Cancer Centre, Melbourne, Victoria 3000, Australia

[2]Sir Peter MacCallum Department of Oncology, The University of Melbourne, Victoria 3010, Australia

[3]The Walter and Eliza Hall Institute of Medical Research, Parkville, Australia.

[4]Department of Medical Biology, The University of Melbourne, Parkville, Australia.

†Co-senior authors.

*Corresponding authors. Email: vervoort.s@wehi.edu.au, ricky.johnstone@petermac.org

Abstract:

Therapeutic targeting of dysregulated transcriptional programs has arisen as a promising strategy for the treatment of leukaemias. The therapeutic response to small molecule inhibitors of Bromodomain-Containing Proteins (BRD), such as BRD2 and BRD4, P300/cAMP-response element binding protein (CBP) and Cyclin Dependent Kinases (CDKs), is generally attributed to the selective disruption of oncogenic gene expression networks driven by enhancers, super-enhancers (SEs) and lineage-specific transcription factors (TFs), including the *c-MYC* oncogene. Using technologies such as thiol (SH)-linked alkylation for the metabolic sequencing of RNA sequencing (SLAM-seq) to profile messenger RNA (mRNA) decay and production rates, we demonstrate that gene intrinsic properties largely govern the selectivity associated with transcriptional inhibition, where total mRNA response signatures are dominated with genes that have short transcript half-lives, including those regulated by SEs and oncogenic TFs. Further highlighting that gene sensitivities only occur in the context of short transcript half-lives, stabilisation of the *c-MYC* transcript through changes in the 3' UTR rendered it insensitive to transcriptional targeting. However, this was not sufficient to rescue *c-MYC* target gene transcription and anti-leukaemia effects following transcriptional inhibition. Importantly, long-lived mRNAs encoding essential genes that evade transcriptional targeting can be rendered sensitive via modulation of mRNA decay kinetics through inhibition of the RNA Binding Protein (RBP), ELAV Like RNA binding protein 1 (ELAVL1)/ Human Antigen R (HuR). Taken together, these data demonstrate that mRNA decay shapes the therapeutic response to transcriptional perturbation and can be modulated for novel therapeutic outcomes using transcriptional agents in leukaemia.

Main body (5000 words)

Introduction

Genetic alterations in cancer can affect proteins involved in almost all regulatory steps of RNA Polymerase II (RNAPII) -driven gene expression. Dysregulated transcription ultimately contributes to cellular transformation and the development of malignant phenotypes (*1*, *2*). This includes leukaemias, where several chromosomal rearrangements, such as those involving the Mixed Lineage Leukemia (MLL) H3K4 methyltransferase, can drive the aberrant expression of leukaemogenic proteins (*3*).

As these transcriptionally dysregulated cancers exhibit a critical dependency on components of the core transcription machinery that regulate RNAPII, small molecule inhibitors that target core transcriptional enzymes and structural proteins have been developed for therapeutic use (*4*, *5*). In leukaemia treatment, this includes compounds that target the transcriptional co-activator p300/cAMP-response element binding protein (CBP), Bromodomain and Extra Terminal (BET) family of epigenetic reader proteins such as Bromodomain-Containing Protein 4 (BRD4) and transcriptional Cyclin Dependent Kinases (t-CDKs) (*6*–*10*).

A large number of publications studying the effects of small molecules targeting the core RNAPII machinery or epigenetic regulatory proteins show that they result in selective gene expression responses. The selectivity is generally attributed to gene-specific chromatin features, including occupancy of the targeted factor, cell-type specific core regulatory transcription factors (CR-TFs), enhancers and super-enhancers (SEs) (*1*, *11*, *12*), all of which impact the *de novo* production of mRNA. In the context of leukaemia this has been described to primarily affect oncogenic networks driven by key TFs such as *c-MYC* (*11*, *13*–*15*). Indeed, the sensitivity of *c-MYC* itself to transcriptional perturbation has largely been associated with a cluster of SEs 1.7 mega bases (Mb) from its transcription start site (TSS) and CR-TFs such as PU.1, MYB and FLI1 (*16*, *17*). Recent work has also demonstrated that co-factors can possess more broad or selective chromatin specificities, including CDK9 and p300/CBP and BRD4, respectively (*12*). Again, both broad and selective cofactor regulatory targets were associated with histone modifications, DNA sequences and TF motifs (*12*).

As the chromatin landscape is the focus in evaluating gene responses to transcriptional therapies, the impact of different stages of the mRNA life cycle to gene expression changes is rarely evaluated. Obtaining information about mRNA life cycle stages can be achieved by leveraging recent technological advances that enable the high-confidence measurement of mRNA production and decay rates genome-wide. This involves metabolic labelling of RNA with the nucleotide analog 4-thiouridine (4sU), and its quantification using affinity- or conversion-based technologies (*18*–*23*). For example, thiol (SH)-linked alkylation for the metabolic sequencing of RNA (SLAM-seq) is a conversion-based approach that uses 4sU dependent thymine-to-cytosine (T > C) conversions for the *in silico* separation of newly synthesized and pre-existing transcripts (*18*).

Using SLAM-seq to assess mRNA kinetics, we demonstrate that transcript decay rates largely dictate the response to transcriptional and epigenetic therapies. Importantly, we further highlight that genetic and small-molecule modulation of mRNA half-lives can alter the effects on transcript levels seen following inhibition of mRNA production and can provide enhanced anti-cancer responses when combined with agents that perturb the core RNAPII machinery.

Results

The anti-leukaemia responses to transcriptional inhibition occurs concomitantly with selective reduction in total mRNA levels

To investigate the role of mRNA kinetics in shaping responses to agents that perturb cofactors with selective (p300/CBP and BRD4; class II) and broad (CDK9 and RNAPII; class I) chromatin specificities (*12*), the biological response to small molecule inhibitors of p300/CBP (A-485), BRD4 (JQ1), CDK9 (AZ-5576) and RNAPII (actinomycin-D; ACTD) in the K562 Chronic Myeloid Leukaemia (CML) cell line was first assessed (Fig. 1A and S1). All agents reduced the

number of K562 cells grown *in vitro* in a concentration and time-dependent manner (Fig. S1A). Moreover, the small molecule concentrations used to assess the anti-leukaemic effects were consistent with on-target activities, as demonstrated by a reduction in H3K18ac, c-MYC protein and RNAPII carboxy-terminal domain (CTD) Serine 2 (Ser2) phosphorylation following treatment with A-485, JQ1 and AZ-5576, respectively (Fig. S1. B) (*8*, *24*, *25*). Using the same leukaemia model and small molecule inhibitors, SLAM-seq was next performed to evaluate responses to transcriptional targeting (*18*) (Fig. 1A-B). Differential gene expression analysis (DGEA) of total mRNA read counts revealed that all transcriptional inhibitors affected the levels of only a subset of expressed genes (Fig. 1C, S2. A). Consistent with previous studies (*26*, *27*), 785 SE-associated genes defined using publicly available H3K27ac ChIP-seq data in K562 cells (Fig. S2. B) and 83 CR SE-associated TFs identified using the Coltron algorithm (Fig. S2. C-D) were significantly more down-regulated compared to all other genes across all treatments (Fig. 1D, S2. E-F). Transcripts repressed following treatment with A-485, JQ1, AZ-5576 and ACTD were enriched for genes encoding several cancer and inflammatory hallmark pathways, including c-MYC targets and cytokine signalling, respectively (Fig. S2. G). This selectivity was observed despite A-485, JQ1, AZ-5576 and ACTD causing largely distinct total mRNA changes, whereby CDK9i and ACTD signatures co-clustered and exhibited the highest degree of similarity (Fig. S2. H). However, the vast majority of genes were refractory to changes in total mRNA levels at these timepoints and inhibitor concentrations (Fig. 1C), including several SE associated genes and CR TFs (Fig. S2. E-F). Overall, these data validate that on the total mRNA level, transcriptional targeting largely perturbs the expression of SE- and CR-TF oncogenic gene networks.

Nascent and total mRNA responses to transcriptional inhibition are disconnected

To investigate whether selective changes in total mRNA levels following small molecule inhibition of p300/CBP, BRD4, CDK9 and RNAPII are due to a concordant change in mRNA production, DGEA was performed on nascent read counts (Fig. 1B). In contrast to the effect seen on total mRNA (Fig. 1C, S2. A), nascent mRNA was more broadly repressed in response to all inhibitors (Fig. 1E, S3. A-C). The greatest effect on nascent mRNA expression was observed following treatment with AZ-5576 and ACTD and globally down-regulated the *de novo* mRNA synthesis of > 80% of genes (Fig. 1E, S3. A-C). In contrast, transcriptional inhibition with p300/CBPi and BRD4i, was selective and significantly reduced the mRNA synthesis of < 50% of expressed genes (Fig. 1E, S3. A-C). Importantly, changes in nascent gene expression with class II inhibitor treatment was still significantly greater in comparison to associated total mRNA changes (Fig. S3. C). In agreement with these data, comparison between nascent and total mRNA read counts revealed only a modest Pearson's correlation coefficient (Fig. S3. D). Correlations were lower with class I inhibitors (0.17-0.3) in comparison to more selective transcriptional perturbation with class II compounds (0.43-0.46) (Fig. S3. D). As an example of the disconnect between changes in nascent and total mRNA abundance, genes such as *HPRT1* that were the least responsive (P-value > 0.05, -0.25 < logFC < 0.25; 200 genes closest to the mean logFC) to changes in total mRNA had significantly down-regulated nascent gene expression, especially in response to class I compounds (Fig. 1F, S3. E). In contrast, the proto-oncogene *c-MYC* was amongst the most responsive to transcriptional perturbation (top 200 genes most significantly down-regulated) on both total and nascent mRNA levels (Fig. 1F, S3. F). This highlights that in a subset of genes, down-regulation of *de novo* mRNA synthesis can result in a concomitant reduction in total mRNA. However, despite global down-regulation of nascent transcripts, most genes appear to be refractory to changes in total mRNA following acute transcriptional inhibition. Taken together, these data suggest that selective targeting of mRNA production is more limited than currently appreciated and infrequently translates into alterations in the global mRNA pool. Moreover, it further indicates that other parameters that define total mRNA levels underpin the observed responses to transcriptional perturbation.

Gene-intrinsic mRNA decay properties shape the response to transcriptional inhibitors

138 Total transcript levels are critically determined by the decay component of the mRNA life-
139 cycle (*28*). To investigate whether mRNA stability influences changes in total mRNA levels following
140 transcriptional inhibition, 4sU pulse-chase combined with SLAM-seq was performed in K562 cells
141 (Fig. 2A), with a concentration of 4sU that retained viability (Fig. S4. A) and proliferation (Fig. S4. B)
142 throughout the experiment. This enabled the generation of estimated mRNA half-life ($t_{1/2}$) parameters
143 for 6580 genes (Fig. S4. C), including for short-lived genes such as *c-MYC* ($t_{1/2}$ = 1.3 hours) (Fig. S4.
144 D), which were concordant with published decay measurements obtained in K562 cells with
145 conversion-based protocols (Fig. S4. E) (*20*, *29*). Functional annotation of genes according to their
146 mRNA half-lives in combination with mRNA production rates, obtained using transient transcriptome
147 (TT) -seq (*21*), revealed that leukaemogenic proteins, namely CR-TFs, were highly labile (Fig. 2B,
148 S4. F). Similarly, high-expression of genes encoding only short-lived mRNAs correlated with poorer
149 Acute Myeloid Leukaemia (AML) patient overall survival (Fig. S4. G-J). These data therefore suggest
150 that fast mRNA kinetics are associated with oncogenes that are clinically relevant for AML.
151 In light of our observation that transcripts within these oncogenic networks are rapidly turned
152 over through a cycle of rapid production and decay (Fig. 2B, Fig. S4. F), we hypothesized that gene-
153 intrinsic parameters are the causative factor driving selective total transcriptional changes to
154 perturbation of the core-transcriptional machinery. Indeed, the most responsive genes to class I and
155 II inhibitors had half-lives approximately 3-4 times shorter than those least responsive to RNAPII-
156 targeting, and the median half-life of each category varied little between class I- or II- mediated
157 transcriptional inhibition (Fig. 2C). Conversely, genes with short mRNA half-lives were significantly
158 down-regulated in comparison to longer-lived gene groups on the total mRNA level with all
159 compounds tested (Fig. S5. A) and were enriched for genes defined as the most responsive (Fig.
160 S5. B). This was more evident with class I compounds, where >90% of most responsive genes were
161 in the shortest $t_{1/2}$ group (Fig. S5. B). In contrast, genes that were least responsive to RNAPII-
162 targeting were over-represented for longer $t_{1/2}$ gene categories (Fig. S5. C), indicating that transcripts
163 with slow decay kinetics maintained total mRNA levels following acute transcriptional inhibition. In
164 addition, mRNA production rates were predictive of total mRNA down-regulation following
165 transcriptional inhibition only in the context of transcript half-lives, where genes with the highest
166 mRNA production rates (pentile 5; 4.2e-02- 6.7 FPKM h^{-1}) and shortest half-lives (pentile 1; $t_{1/2}$ 0.9-
167 3.3 hours) were most strongly repressed following treatment with transcriptional inhibitors (Fig. S5.
168 D). Moreover, the most-responsive genes (Fig. 1F) were enriched (25.5-37%) in the shortest lived
169 and most highly produced subset (Fig. S5. D), where this was not observed for genes least-
170 responsive (Fig. 1F, S5. E).
171 To quantitatively assess the impact of transcript half-lives to total mRNA abundance upon
172 transcriptional inhibition *in silico*, we developed a mono-exponential model of steady state gene
173 expression using only mRNA production and decay rates (Fig. S5. F). Production rates (k_1) and
174 decay rates (k_2) were determined using TT-seq and SLAM-seq (Fig. 2A) measurements obtained in
175 K562 cells, respectively. Predicted steady state mRNA levels significantly correlated with
176 experimental measurements of baseline mRNA abundance (Fig. S5. G), indicating that the model
177 was sufficiently accurate to estimate equilibrium mRNA levels with a variety of initial conditions and
178 time intervals. *In silico* modelling of total mRNA abundance following two hours of complete
179 abrogation of *de novo* mRNA synthesis (Fig. S5. F, H) and subsequent functional analysis, revealed
180 significant negative enrichment of TFs, cytokine signalling, inflammatory and *c-MYC* target cancer
181 hallmark pathways and SE-transcriptional programs, where oncogenes such *c-MYC* were amongst
182 the most reduced (Fig. 2D, S5. I-J). This is in line with data obtained using total mRNA changes to
183 small molecules targeting RNAPII (Fig. 1C, S2. G). Consistently, comparison of *in silico* transcription
184 shutdown and experimental total mRNA measurements revealed highly similar and significant gene
185 expression changes, albeit more strikingly with class I inhibitors (Fig. S5. K). In agreement with these
186 results, short mRNA $t_{1/2}$ genes were strongly predicted to be more responsive to RNAPII targeting,
187 where predictive accuracy was higher with class I inhibitors (AUC 0.93-0.94) in comparison to class
188 II (AUC 0.86-0.90) (Fig. 2E). This firstly highlights that any change in total mRNA levels following

189 global perturbation of mRNA production with class I inhibitors is strongly determined by mRNA half-
190 lives. Secondly, these data also suggest that changes in total mRNA levels of distinct genes affected
191 by class II compounds stems from a combination of selective inhibition of *de novo* mRNA synthesis
192 and gene intrinsic mRNA $t_{1/2}$. Whilst reciprocal adjustments in mRNA synthesis and decay rates to
193 maintain total cellular mRNA concentrations can occur, a phenomenon called 'transcriptional
194 buffering', modelling of complete transcriptional shutdown using treatment-specific mRNA decay
195 rates (Fig. S6. A-D) correlated significantly with experimentally measured total mRNA changes (Fig.
196 S6. E). This indicates that transcriptional buffering does not negate the importance of mRNA decay
197 rates in shaping the total mRNA response to the class of therapeutic transcriptional inhibitors.
198 Analysis of an independent SLAM-seq dataset from K562 cells (Fig. S7. A-D) (*19*) revealed
199 that transcript half-life also defines the response to transcriptional disruption through small molecule
200 inhibition of BRD4 or CDK9, as well as, acute protein degradation of c-MYC and BRD4 (Fig. S7. E-
201 I). In addition, short-lived transcripts were most sensitive to inhibition of BCR-ABL1 signalling using
202 nilotinib (Fig. S7. E-I). Concordant with our observations using K562 cells, the magnitude of nascent
203 mRNA responses greatly exceeded those on the total mRNA level, indicating that transcript stability
204 regulates this response, which has therapeutic implications. To extend our findings to another
205 leukaemic model, we measured mRNA decay parameters (Fig. S8. A-B) and transcriptional
206 responses to various small molecule transcriptional inhibitors (Fig. S8. C-D) in MLL-rearranged THP-
207 1 cells. Moreover, we also included an independent and previously published SLAM-seq dataset
208 assessing responses to transcriptional perturbation in THP-1 cells in our analysis (Fig. S8. C-D) (*30*).
209 This revealed that similar to K562 cells, the total mRNA response in THP-1 cells to distinct BET,
210 CDK9, CDK12/13 and CDK7 inhibitors was largely dependent on gene-intrinsic decay properties,
211 where a much larger transcriptional response on the nascent mRNA level was observed (Fig. S8. E-
212 H).
213 Taken together, these data demonstrate that mRNA decay parameters can isolate a group
214 of responsive genes to all forms of transcription abrogation in manner that is completely agnostic to
215 the chromatin landscape or the molecular consequences of the cofactor targeted.
216
217 ***MAC-seq defines the role of mRNA decay properties to changes in gene expression with 73***
218 ***epigenetic and transcriptional compounds***
219 To assess the role of mRNA $t_{1/2}$ parameters to gene expression responses across a wider
220 range of clinically relevant inhibitors, we used Multiplexed Analysis of Cells sequencing (MAC-seq)
221 to profile total mRNA changes in response to 73 small molecule inhibitors targeting epigenetic and
222 transcriptional proteins in K562 cells, where previously tested drugs (Fig. 1A) were included as
223 controls (Fig. 3A, S9. A). DGEA revealed a number of differentially expressed events (Fig. 3B), where
224 only eight out the 73 compounds tested globally repressed transcription and significantly down-
225 regulated > 1000 genes (Fig. 3C). This first group of inhibitors (class I) target cofactors described to
226 exhibit broad chromatin specificities (*12*), including those able to perturb t-CDKs and the core RNAPII
227 machinery (Pan-Tx) (Fig. 3C, S9. A). Moreover, a second group (class II) of an additional six drugs
228 targeting BRD4, p300/CBP, histone deacetylases (HDACs), and protein phosphatases (PP), were
229 able to selectively down-regulate a subset of least 200 genes, consistent with their role as regulating
230 only a part of the genome (*12*) (Fig. 3C, S9. A). Despite technical and experimental differences
231 between the MAC- and SLAM-seq protocols, MAC-seq total mRNA data recapitulated the previous
232 segregation of the tested compounds into class I and II (Fig. 1A, 3C). Remaining compounds, defined
233 as class III, that targeted histone demethylases (HDMe) and methyltransferases (HMe), DNA alkyl-
234 (DNA AGT) and methyl- transferases (DNAMe), sirituin (SIRT), PARP, ELAVL1/HuR and
235 topoisomerases (Topo) either repressed the expression of a minimal number of genes (< 200) or
236 primarily up-regulated transcription (Fig. 3C). This indicates that gene-intrinsic mRNA stability most
237 likely has minimal influence on the total transcriptome for class III compounds.
238 Uniform Manifold Approximation and Projection (UMAP) of drug treatments revealed that gene
239 changes grouped according to drug treatment (Fig. S9. B, *middle*), drug protein target (Fig. S9. B,

240 *bottom*) and family (Fig. 3D, *top*) and class (Fig. 3D, *middle*). Notably, despite all class I compounds
241 forming an entirely distinct cluster (Fig. 3D, *middle*), more detailed analysis of this drug class in an
242 isolated setting revealed separation between Pan-Tx, CDK9/7/12/13 and CDK11/12/13 inhibitors
243 (Fig. 3D *bottom*, S9. A). This suggests that though class I compounds are able to broadly repress
244 gene expression, they are mechanistically distinct and not equivalent. Inhibitors within the class II
245 category however, with the exception of drugs targeting BET proteins, clustered separately (Fig. 3D
246 *bottom*, S9. A), highlighting that they induce distinct and selective transcriptional responses in line
247 with previously defined chromatin specificities (*12*).
248 Data from figure 2 demonstrated that mRNA decay is a critical determinant to changes in total
249 gene expression following transcription inhibition with p300/CBPi, BRD4i, CDK9i and ACTD, so it
250 was determined if these findings could be extended to other compounds able to globally (class I) or
251 selectively (class II) repress gene expression as defined by MAC-seq (Fig. 3C). Genes most
252 responsive (top 200 genes most significantly down-regulated) to class I and II inhibitors were
253 significantly shorter lived in comparison to genes least responsive (P-Value > 0.05, -0.25 < logFC <
254 0.25; 200 genes closest to the mean logFC) to transcriptional targeting (Fig. 3E, S9. C). The
255 difference in half-life between most and least responsive gene sets was most striking with class I
256 inhibitors, where mRNA stability varied up to three-fold between the two categories (Fig. 3E, S9. C).
257 Consistently, the most short-lived genes, as defined previously in Fig. 2, were enriched as genes
258 most responsive to transcriptional targeting by class I and II inhibitors (Fig. 3F). This was more
259 evident with class I compounds, which had > 40% of most-responsive genes within the most short-
260 lived group (Fig. 3F). In agreement with these data, short-lived mRNAs were more significantly
261 depleted amongst highly abundant transcripts in response to class I compounds in comparison to
262 class II and III mRNAs (Fig. S9. E). In contrast, the most long-lived genes were enriched in genes
263 least-responsive to targeting by most inhibitors within the two classes (Fig. S9. D) and as a
264 consequence were found to be significantly over-represented across the most abundant mRNAs in
265 responses to class I and II compounds compared to class III (Fig. S9. F). Furthermore, genes with
266 short half-lives were highly predictive as genes amenable to t-CDK and general RNAPII inhibition
267 using models of complete transcription shutdown (Fig. 3G), consistent with previous findings (Fig.
268 2E). Due to selective targeting observed on the nascent mRNA level and longer drug incubation
269 times, predictive accuracy was modest with BRD4, p300/CBP, pan-HDAC and PP targeting (Fig.
270 3G). Taken together, these data demonstrate that the role of mRNA decay can be extended to
271 several transcriptional and epigenetic inhibitors, where both selective and global down-regulation of
272 gene expression is strongly dictated by gene intrinsic mRNA $t_{1/2}$ parameters.
273
274 ***c-MYC mRNA stabilization does not rescue biological and transcriptional effects of***
275 ***transcriptional targeting***
276 A putative common effector mechanism of small molecules that inhibit mRNA production in
277 leukaemia is repression of *c-MYC* (*13*). In K562 cells, *c-MYC* is necessary for driving the expression
278 of a conserved set of gene targets encoding proteins necessary for nucleotide biosynthesis (*11*).
279 Having determined that *c-MYC* itself and its target genes were short lived, we sought to assess
280 whether altered *c-MYC* decay kinetics could modulate responses to transcriptional inhibition. As *c-*
281 *MYC* stability is regulated by AU-rich elements (AREs), AUUUA and miRNA recognition motifs within
282 its 3'UTR (*31–35*), CRISPR/Cas9 -mediated homology directed repair (HDR) in K562 cells was used
283 to substitute the *c-MYC* endogenous 3'UTR for the 3' region of the longer-lived gene *HPRT1* with a
284 destabilized GFP (dsGFP) reporter, termed '*c-MYC-HPRT1* 3'UTR' (Fig. 4A). Designated as '*c-MYC*-
285 control 3'UTR', dsGFP was knocked-in 5' of the endogenous *c-MYC* 3'UTR sequence as a control
286 cell line (Fig. 4A). Both cell models were validated by PCR (Fig. S10. A-F) and sequencing (Fig. S10.
287 G-H) using primers complementary to various regions of the *c-MYC* locus. As our system genetically
288 engineered the endogenous 3'UTR of *c-MYC*, its genomic location, in addition to *cis*- and *trans*-
289 factors that impact its regulation remained unaffected. This therefore enables the direct assessment
290 of altered mRNA stability to transcription targeting within the endogenous chromatin context.

291 Assessment of mRNA stabilities demonstrated that knock-in of the *HPRT1* 3'UTR increased the half-
292 life of the chimeric *c-MYC* transcript by approximately eight hours following treatment with ACTD,
293 representing a four-fold increase over the half-life of the endogenous and entopic *c-MYC* transcripts
294 (Fig. 4B, S11. A-B). Moreover, *c-MYC* transcript stabilisation did not alter baseline *c-MYC* total
295 mRNA abundance (Fig. S11. C), in contrast to nascent mRNA levels, where it was significantly lower
296 in comparison to the control (Fig. S11. D).
297 To further investigate the response of stabilized *c-MYC* to RNAPII targeting, c-*MYC*-control
298 and -*HPRT1* 3'UTR cell lines were treated with the class I compounds AZ-5576 (CDK9i) or ACTD
299 for six hours and whole transcriptome RNA-Seq was performed. Consistent with previous findings
300 (Fig. 1, 3), DGEA of exon and intron reads revealed a global decrease in total and nascent gene
301 expression, respectively (Fig. S11. E-G). Whilst de *novo c-MYC* synthesis was significantly down-
302 regulated irrespective of *c-MYC* mRNA half-life (Fig. 4C *right*), *c-MYC-dsGFP* total mRNA (Fig. 4C
303 *left)* and protein abundance (Fig. 4D, S11. H-K) revealed that *c-MYC* stabilization rendered it less
304 sensitive to targeting by either compound. The resistance to RNAPII targeting on the total mRNA
305 level was *c-MYC* specific, as *c-MYC* was the most significantly altered gene with each treatment
306 (Fig. 4E) and clustering of total mRNA changes highlighted that conditions grouped according to
307 inhibitor and not cell line (Fig. S11. L). Consistently, correlation analysis of all DEGs in c-*MYC*-control
308 and -*HPRT1* 3'UTR cell lines with CDK9i and ACTD revealed that changes were highly similar and
309 significant (Pearson's correlation coefficient 0.96-0.97, P-Value < 2.2e-16) (Fig. S11. M).
310 Remarkably, increasing *c-MYC* mRNA half-life through swapping of the endogenous *c-MYC*
311 3'UTR with that of *HPRT1* did not rescue the expression of previously defined *c-MYC* target genes
312 (Fig. S11. N-O) (*11*). Although nascent *c-MYC* target gene expression was significantly less down-
313 regulated with CDK9i treatment in the c-*MYC-HPRT1* 3'UTR cell line (Fig. S10. N), it was not
314 sufficient to prevent reductions in total mRNA (Fig. S10. N). In line with these data, the proliferation
315 and survival between K562 c-*MYC*-control and -*HPRT1* 3'UTR cell lines was not altered upon CDK9i
316 and ACTD treatment *in vitro* (Fig. 4F).
317 Taken together, these data suggest that class I inhibitors can mediate anti-leukemic effects
318 even when expression of a key target gene, *c-MYC*, is maintained due to prolonged mRNA half-life.
319 This challenges the notion that loss of *c-MYC* expression is necessary for the biological and
320 molecular consequences of perturbing nascent mRNA synthesis using agents such as AZ-5576 or
321 ACTD. Therefore, the observation that *c-MYC* repression is the effector mechanism upon inhibition
322 of transcriptional proteins in leukaemia is not due to specific targeting of *c-MYC* SEs and CR-TFs,
323 but rather a consequence of short transcript half-lives. Gene-intrinsic mRNA decay properties are
324 thus a key determinant in establishing gene responsiveness, such as that of *c-MYC*, to compounds
325 that target RNAPII driven gene expression, and without which, selective responses would not be
326 found with most transcriptional compounds.
327
328 ***Selective modulation of mRNA decay through ELAVL1 targeting***
329 Having established that the therapeutic response to transcriptional inhibition is shaped by
330 mRNA decay kinetics, we next investigated whether mRNAs with long half-lives and consequently,
331 not amenable to perturbation, could be sensitised to RNAPII targeting in leukaemia. We therefore
332 re-analyzed our previously published genome-wide CRISPR-Cas9 knockout screening datasets
333 performed in AML cell lines treated with CDK9i, with a focus on RBPs due to their ability to bind
334 mRNAs at specific sequence motifs to affect mRNA post-transcriptional processing (*36*).
335 The analysis revealed that knockout of 16 RBPs sensitized both THP-1 and MV4;11 AML
336 cell lines to CDK9i (Fig. 5A, S12. A). This included the RBP ELAVL1 (Fig. 5A, S12. A-B), which has
337 been reported to stabilize oncogenic transcripts in AML and promote Leukemic Stem Cell (LSC) self-
338 renewal and survival (*37*, *38*). THP-1 cells with knockout of *ELAVL1* (Fig. 5B) were sensitized to the
339 anti-leukemic effects of AZ-5576 (Fig. 5C-D, S12. C), thereby independently validating the results
340 from the genome-wide screens. Given the proposed oncogenic role of *ELAVL1* (*37*, *38*) it was
341 unsurprising to observe that *ELAVL1* knockout also resulted in a proliferative disadvantage in the

342 absence of any CDK9i treatment (Fig. 5D). This was concomitant with a modest decrease in global
343 total mRNA levels (Fig. S12. D-E) and an enrichment of interferon signalling pathways (Fig. S12. F),
344 in line with previous reports in THP-1 cells and validating our experimental model (*39*).
345 To interrogate the mechanism of CDK9i sensitization mediated by ELAVL1 knockout, THP1
346 ELAVL1 wild-type and knockout cells were treated with CDK9i for six hours and 3'UTR RNA-seq
347 was performed. Consistent with our findings (Fig. 1, 3), DGEA of total read counts revealed a global
348 decrease in total gene expression with CDK9i across both *ELAVL1* wild-type and knockout cell lines,
349 and the magnitude of global transcript down-regulation was modestly greater in ELAVL1 knockout
350 cells (Fig. 5E, S12. D, G). Whilst the CDK9i response between cell lines was similar as demonstrated
351 by co-clustering of samples (Fig. S12. H) and correlation analysis (Pearson's correlation coefficient
352 0.917, P-Value < 2.2e-16) (Fig. S12. I), further investigation revealed 57 genes that were significantly
353 more down-regulated (logFC < -1 and adjusted P Value < 0.01) upon ELAVL1 genetic depletion (Fig.
354 5E, S12. J). As ELAVL1 has been described to regulate mRNA stabilities, the half-lives of the 57
355 transcripts sensitised to CDK9i following *ELAVL1* knockout were assessed. Using previous transcript
356 decay measurements in THP-1 cells (Fig. S7. G), it was evident that whilst the 20% most short-lived
357 mRNAs were enriched in transcripts sensitised in *ELAVL1* knockout upon CDK9i , there was a subset
358 of transcripts with longer half-lives (Fig. 5F *left*). Moreover, incorporation of THP-1 dependency
359 scores obtained from the Broad Institute Depmap Portal demonstrated that sensitised transcripts
360 with longer half-lives were highly essential, such as *NIFK* and *MED29* (Fig. 5F *right,* G). Indeed, both
361 *NIFK* and *MED29* have been associated with oncogenic characteristics in a variety of cancer types
362 (*40*, *41*). Collectively, our findings highlight that leukaemia cell line sensation to CDK9i following
363 *ELAVL1* knockout may be associated with the perturbation of essential mRNAs with long half-lives,
364 which would otherwise be less amenable to transcriptional perturbation in *ELAVL1* wild-type cells.
365 To interrogate the therapeutic potential of ELAVL1 targeting in the context of CDK9i in
366 leukaemia, THP-1 cells were treated with CDK9i in combination with the small molecule MS-444, a
367 potent inhibitor of ELAVL1 (*42*). Importantly, MS-444 has been demonstrated to exhibit single agent
368 efficacy in models of leukameia *in vivo* (*38*). Assessment of cell death revealed that the drug
369 combination resulted in greater cytotoxicity than each inhibitor alone and was highly synergistic (Fig.
370 5H-I, S12. K). These data are in line with our genetic ELAVL1 knockout experiments and suggest
371 that the therapeutic perturbation of the mRNA decay and transcriptional machinery is an actionable
372 and novel combination therapy for the treatment of AML.
373
374 ***Discussion***
375 RNAPII-driven transcription has been therapeutically targeted across solid and
376 haematological malignancies with biological and therapeutic effects proposed to occur through
377 selective perturbation of oncogenic gene networks (*1*, *26*). The current literature suggests that the
378 discrete targeting of selected genes following transcriptional perturbation is mechanistically linked to
379 association with enhancers, SEs and disproportionate occupancy of critical chromatin co-factors,
380 such as BRD4 and TFs, at promotors; however, the role of mRNA stability has not been extensively
381 assessed in this context.
382 Here, we demonstrate that selective and broad targeting of RNAPII-driven transcription by
383 class I and II therapeutic inhibitors, respectively, results in discrete alterations in total mRNA
384 abundance that are defined by transcript decay rates (Fig. 6). Despite our analyses being completely
385 agnostic to the chromatin landscape or the molecular consequences of the core-transcriptional
386 component targeted, they were able to effectively isolate a group of responsive genes to all forms of
387 transcriptional perturbation. Indeed, both class I and II inhibitors reduce the total mRNA levels of
388 genes with short transcript half-lives, several of which are CR TFs, associated with oncogenic
389 signalling pathways or promotor proximal to SEs. Although some studies indicate that these
390 oncogenic networks are particularly sensitive due to reduction of the CR TFs within SE and promotor
391 regions, whether down-regulation of TFs and SE-driven transcription were causally linked remained
392 unclear (*26*, *43*, *44*). Our data indicates that targeting of SE-driven transcription is only possible when

393 the associated gene has short-lived mRNA, and therefore implicates gene-intrinsic mRNA decay
394 parameters in the selective perturbation of SE oncogenic programs. This further highlights that the
395 selectivity of these therapies is very likely over-estimated and suggests that oncogenic networks
396 driven by SEs and short-lived and highly produced CR TFs are intrinsically sensitized to any form of
397 abrogation of *de novo* mRNA synthesis, thus challenging the notion that selective targeting is
398 required to specifically disrupt oncogenic transcription. In contrast, genes with stable mRNAs are
399 largely refractory to transcriptional targeting when assessing total mRNA levels and are functionally
400 related to cellular housekeeping roles (*18*, *45*). This may prove a challenge for the use of
401 transcriptional inhibitors as a therapeutic intervention for leukaemias that exhibit dysregulated
402 metabolic activity or a heightened dependence on metabolic pathways.
403 Interestingly, alterations in mRNA decay frequently occur in cancer, including leukaemias, in
404 either a gene-specific manner or through mutations in mRNA complexes to thus affect global mRNA
405 turnover (*35*, *46–49*). For example, stabilization and the resultant increase in steady state expression
406 of the *PD-L1* transcript frequently occurs in haematological and stomach cancers from mutations
407 that disrupt the *PD-L1* 3'UTR, and in *in vivo* models of lymphoma, leads to immune evasion and
408 decreased survival (*35*). Similarly, c-MYC 3'UTR truncations caused by chromosomal translocations
409 in human T-cell leukaemias (TCL) have been described to increase c-MYC expression via transcript
410 stabilisation (*50*, *51*). In addition to gene-specific truncations of 3'UTR sequences in cancer, mRNA
411 stability can be broadly affected via genetic alterations that impact the mRNA decay machinery and
412 RBPs. This includes loss of function mutations in the Carbon Catabolite Repression—Negative On
413 TATA-less (CCR4-NOT) Transcription subunit 3 (CNOT3) subunit of the CCR4-NOT deadenylase
414 complex in T-cell Acute Lymphoblastic Leukaemia (T-ALL) (*47*) and the 3'-5' exoribonuclease of the
415 exosome complex, DIS3 in MM and RUNX1 -mutated AML (*48*, *49*). Moreover, widespread
416 alternative polyadenylation (APA) in a variety of cancer types has been demonstrated to shorten
417 3'UTRs and increase transcript stability and protein levels (*46*, *52*). Whilst the mechanism of
418 increased APA in cancers is poorly understood, there is evidence that down-regulation APA factors
419 such as CFIm25 and PCF11 may contribute increased APA in certain malignancies (*53*). Based on
420 our observations that long-lived transcripts are resistant to transcriptional inhibition, targeting
421 stabilized oncogenic mRNA in the context of deregulated decay machinery may prove unsuccessful
422 with class I and II therapeutic compounds.
423 Due to the lack of on-target inhibitors, therapeutic inhibition of mRNA decay pathways in the
424 oncology setting remains largely unexplored. The widely utilised chemotherapeutic nucleoside
425 analog 5-flurouracil (5-FU), initially characterised to perturb the DNA synthesis regulator thymidylate
426 synthase, has been also reported to perturb the exosome subunit EXOSC10 (*54*, *55*). Moreover,
427 small molecule inhibition of the scavenger mRNA de-capping enzyme DCPS using RG3039 in pre-
428 clinical AML models affected pre-mRNA splicing, rather than cytoplasmic decay pathways to elicit
429 cytotoxic effects (*56*). An alternative approach to alter transcript decay in cancer for therapeutic
430 benefit has been to target RBPs that promote oncogenic mRNA stability. In the leukaemia setting,
431 recent work has demonstrated that the ELAVL1 inhibitor MS-444 destabilises the mitochondrial
432 import protein TOMM34 and hampers LSC-driven leukaemic reconstitution *in vivo* (*38*). In line with
433 these findings, we observe that genetic knockout and therapeutic inhibition of ELAVL1 limits THP-1
434 cell line growth. Targeting mRNA decay pathways directly or through RBPs is of high clinical
435 significance, particularly because long-lived transcripts not amenable to transcriptional inhibition
436 encode for proteins that regulate cellular homeostasis and metabolism. Indeed, aberrant metabolism
437 is recognised as a cancer hallmark and is central to leukaemia cell survival and proliferation (*57*, *58*).
438 This is supported by pre-clinical studies in leukaemia models showing that small molecule inhibition
439 of various metabolic pathways as a highly promising avenue for leukaemia therapy (*58*). Efforts to
440 destabilise long-lived mRNAs may therefore be an alternative approach to perturb oncogenic
441 metabolism.
442 Having observed that a large number of mRNAs are not sensitive to transcriptional
443 perturbation due to their long half-lives, we demonstrated that combination therapy with a transcript

destabilizing agent such as MS-444, provides a novel opportunity to target genes that were otherwise impervious to RNAPII targeting. Whilst we demonstrated that 57 transcripts were significantly sensitised with ELAVL1 knockout upon CDK9i treatment, only a minority possessed long half-lives. As knockout of ELAVL1 has been demonstrated to alter mRNA decay rates, our half-life measurements, derived from THP-1 cells with wild-type ELAVL1, may under-estimate the number of transcripts with short mRNA decay kinetics (*59*).

Overall, this study highlights the importance of mRNA decay parameters in governing total gene expression levels in response to selective and global inhibitors of RNAPII -driven transcription, and provides novel mechanistic insight that can be leveraged for therapeutic benefit. Moreover, our work shifts the paradigm that selective responses observed in these contexts are largely driven by selective abrogation of mRNA synthesis as a result of particular genomic determinants but rather demonstrates that these largely result from gene-intrinsic mRNA properties.

456 ***Methods***

457 Cell lines and culture

458 K562 CML parental and HDR-edited and THP-1 AML parental and inducible knockout cells were
459 cultured in Roswell Park Memorial Institute (RPMI) medium (Thermo Fisher Scientific, Waltham, MA,
460 USA, 11875093) containing 10% (v/v) heat-inactivated fetal bovine serum (HI-FBS; Thermo Fisher
461 Scientific, 10099), penicillin (100 U/ml), streptomycin (100 µg/ml) (Thermo Fisher Scientific,
462 15140122) and 2 mM GlutaMAX (Thermo Fisher Scientific, 35050061) at 37°C and 5% carbon
463 dioxide. HEK293T cells were cultured in Dulbecco's Modified Eagle's Medium (DMEM; Thermo
464 Fisher Scientific, 11995073) containing 10% (v/v) heat-inactivated fetal bovine serum (HI-FBS;
465 Thermo Fisher Scientific, 10099), penicillin (100 U/ml) and streptomycin (100 µg/ml) (Thermo Fisher
466 Scientific, 15140122) at 37°C and 10% carbon dioxide. Drosophila melanogaster S2 cells were
467 cultured Schneider's *Drosophila* medium (Thermo Fisher Scientific, 21720) supplemented with 10%
468 HI-FBS, penicillin (100 U/ml), streptomycin (100 µg/ml), and 2 mM GlutaMAX at room temperature
469 and atmospheric carbon dioxide. Cell lines for all assays were seeded at 50-70% confluency the day
470 prior unless otherwise indicated.
471
472 Compounds

473 See supplementary tables 1 and 2.
474
475 Generation of ELAVL1 inducible knockout cell lines

476 Independent sgRNAs targeting ELAVL1 (*69*) and non-targeting sgRNA controls (SCR;
477 supplementary table 3) flanked with BsmBI overhangs were ligated into the vector FgH1tUTG-GFP
478 (Addgene Plasmid #70183) using 1uL BsmBI (New England Biolabs, R0739) in NEBuffer 3.1 (New
479 England Biolabs, B7203S). This was similarly performed for SCR sgRNA cloned into the vector
480 FgH1tUTG-BFP (*47*). Cloned FgH1tUTG vectors, pMDLg/pRRE (Addgene Plasmid #12251), pRSV-
481 Rev (Addgene Plasmid #12253) and pVSV.G (Addgene Plasmid #12259) third generation lentiviral
482 vectors were transiently transfected into HEK293T cells using polyethylenimine (PEI; 1µg/mL; 25kD
483 linear; BioScientific Pty Ltd, 23966). Following 48 hours, viral supernatant was harvested and filtered
484 using a 0.45µM filter. Viral supernatant was added THP-1 cells constitutively expressing S.*pyogenes*
485 Cas9 (FUCas9-Cherry vector; Addgene Plasmid #70812) prior to transduction using sequa-brene
486 (4µg/mL; Sigma Aldrich, S2667-1VL) and centrifugation at 500g for 4 minutes at room temperature
487 (*47*). Expanded cells were sorted for populations expressing cherry and GFP or BFP using Becton
488 Dickinson (BD) Fussion 3 or 5 sorters. sgRNA expression was induced using doxycycline (1µg/mL;
489 Sigma Aldrich, D9891). All experiments were performed four days following doxycycline induction
490 unless otherwise indicated.
491
492 CRISPR HDR generation of MYC transcript stable clones

493 Parental K562 cells (5e+05) were washed in Phosphate Buffered Saline (PBS) twice and
494 resuspended in Cell Line Nucleofector solution SF (16.4uL) with Supplement (3.6uL) (SF Cell Line
495 4D-nucleofector X Kit, Lonza, V4XC-2032). Alt-R SpCas9 nuclease (100pmol, Integrated DNA
496 Technologies, 1074182), single guide RNAs (sgRNAs) targeting the c-MYC stop codon and 3' end
497 of its 3'UTR (300pmol, supplementary table 3) and pUC57 or pUC57-Mini donor plasmid (1000ng;
498 GenScript Gene Sythesis) containing recombinant sequences for dGFP, P2A cleavable peptide and
499 HPRT1 or c-MYC 3'UTRs, respectively (supplementary table 4), were incubated together for 20
500 minutes at room temperature, prior to being placed on ice. Ribonucleoprotein (RNP) complex (5uL)
501 was added to the cell suspension (20uL), 20uL of which was subsequently transferred to 16-well
502 Nucleocuvette Strip and electroporated using the 4D-Nuceleofector X unit (program FF120, Lonza,
503 AAF-1002X). Warmed culture medium (100uL) was added to cell suspension and incubated at 37°C
504 and 5% carbon dioxide for 10 minutes. Cell suspension was then transferred to a 24-well cell culture
505 plate containing culture medium (1mL) and IDT Alt-R HDR electroporation enhancer (20uM;
506 Integrated DNA Technologies, 1081073) and incubated at 37°C and 5% carbon dioxide for 24 hours,

507 after which cells were washed twice with fresh culture medium and cultured at 37°C and 5% carbon
508 dioxide. After expansion, cells were sorted and enriched for GFP positivity three successive times,
509 followed by isolation of single cells into 96-well culture plates using Becton Dickinson (BD) FACSAria
510 Fusion 3 or 5 Cell Sorters. Three clones with successful knock in of each donor vector were identified
511 with KAPA HiFi (Roche, 7958935001) using isolated genomic DNA (DNeasy Blood & Tissue Kits
512 (Qiagen, 69506) and primers designed outside or within plasmid homology arms (supplementary
513 table 5). PCR fragments were subsequently separated using agarose gel electrophoresis (see
514 below). Knock-in sequence was validated using Sanger sequencing of PCR fragments detailed
515 above at the Australian Genome Research Facility (AGRF). Total-RNA sequencing was performed
516 using a single representative clone of each knock-in.
517
518 Propidium Iodide, 4′,6-diamidino-2-phenylindole and Cell Trace Violet staining
519 For cell viability and proliferation studies using propidium iodide (PI) and/or Cell Trace Violet staining,
520 respectively, cells (1 x10^7) were centrifuged (500g at 4°C for 4 minutes), resuspended in PBS
521 supplemented with 0.1% (w/v) BSA and stained with 5μM CTV dye (Thermo Fisher Scientific,
522 C34557) in a 37°C water bath for 10 or 20 minutes. Five volumes of ice-cold culture medium was
523 added to cell suspension to quench unbound dye. Cells were then centrifuged (500g at 4°C for 4
524 minutes), resuspended in PBS supplemented with 2% (v/v) HI-FBS, sorted for a narrow peak of
525 CTV-positivity on BD FACSAria Fusion 3 or 5 Cell Sorters. Following treatment, CTV-stained or
526 unsustained cells were resuspended in PBS containing 1μg/mL PI (Sigma Aldrich, P4170).
527 For cell viability studies using 4′,6-diamidino-2-phenylindole (DAPI), cells were treated with AZ-5576
528 (CDK9i) for 72 hours, centrifuged (500g at 4°C for 4 minutes) and resuspended in PBS containing
529 1μg/mL DAPI (Sigma Aldrich, D9542-100MG). Analysis of flow cytometric data was preformed using
530 the BD Fortessa X20 and FlowJo v10 software (Ashland). ZIP synergy scores were determined and
531 visualised using synergyfinder (v3.0.1) on Rstudio (v4.0.2).
532
533 Total cell number quantification
534 Absolute cell number was determined with the addition of 1×10^4 calibration beads directly to cells
535 prior to analysis. 0.2 μM Propidium iodide (PI) was also added with the beads to identify dead cells
536 by exclusion. Ratio of live cells to beads was measured by flow cytometry to determine the absolute
537 live cell number in cell culture.
538
539 Intracellular staining of c-MYC
540 Intracellular staining of Myc was performed as previously described (*60*). Briefly, cells were
541 harvested at the timepoints indicated and were immediately resuspended in fixation buffer (0.5%
542 paraformaldehyde, 0.2% Tween-20 and 0.1% bovine serum albumin in PBS) at room temperature,
543 for at least 24 hours until staining was performed. Fixed cells were stained with either anti-Myc (clone
544 D84C12, Cell Signalling Technology) or a rabbit IgG isotype-matched control antibody (clone D1AE,
545 Cell Signalling Technology) before staining with an anti-rabbit IgG conjugated to Alexa Fluor 647.
546 Staining of all fixed samples within one experiment was performed at the same time.
547
548 Cell competition assays
549 Four days after induction of sgRNA using doxycycline (1μg/mL; Sigma Aldrich, D9891), THP-1 Cas9
550 cells expressing FgH1tUTG-GFP constructs were mixed at a 1:1 ratio with THP-1 Cas9 cells
551 expressing a SCR sgRNA in the FgH1tUTG-BFP backbone. Cells were cultured in the presence of
552 DMSO or AZ'5576 (CDK9i; 10nM and 100nM). The BD LSR Fortessa Flow Cytometer was used to
553 assess the relative proportions of GFP- and BFP-positive cells following mixing (time point 0) and at
554 time points indicated.
555
556 Agarose gel electrophoresis and gel imaging

557 Blue/orange loading dye 6X (Promega, G1881) was added to PCR fragments, which were
558 subsequently separated using 1% agarose gels prepared with molecular grade agarose (Bioline,
559 BIO-41025), Tris base- acetic acid- EDTA (TAE) 1X solution and SYBR Safe DNA Gel Stain (Life
560 Technologies, S33102). Agarose gels were imaged on the GelDoc XR+ Imager (BioRad) using
561 ImageLab Software (BioRad).
562
563 Quantitative PCR and analysis
564 Cells (1e+06 per time point) were incubated with 1ug/mL ACTD at 37°C and 5% carbon dioxide,
565 harvested 0-, 2-, 4- and 8- hours post-treatment, centrifuged (1400rpm at 4°C for 4 minutes), washed
566 in ice-cold PBS and resuspended in 300uL TRIzol (Thermo Fisher Scientific, 15596026). RNA was
567 extracted from lysates using the Direct-zol RNA MiniPrep Kit (Zymo Research, R2052) and
568 complimentary DNA (cDNA) was synthesised (from 1ug RNA) using the Applied Biosystems High
569 Capacity cDNA Reverse Transcription Kit (Thermo Fisher Scientific, 4368814). Quantitative PCR
570 (qPCR) was performed using cDNA, 0.25uM forward and reverse oligo primers (see supplementary
571 table 6) and SensiFAST SYBR Hi-ROX Kit (Bioline, BIO-92005) in 384-well plates with the
572 LightCycler 480 Instrument II (Roche, 05015243001). Threshold cycles for each reaction were
573 analysed using the $\Delta\Delta C_t$ method normalising to GAPDH as the housekeeping gene.
574
575 SDS-polyacrylamide gel electrophoresis and western blotting
576 Cells (1e+06) were washed in PBS, lysed in Laemelli Buffer (60 mM tris-HCl (pH 6.8), 10% (v/v)
577 glycerol, and 2% (w/v) SDS) and incubated at 95°C for 10 minutes. Lysate protein concentration was
578 determined using the Pierce BCA Protein Assay Kit (Thermo Fisher Scientific, 23225) and
579 absorbance at 562nm wavelength was measured on the iMark Microplate Absorbance reader
580 (BioRad) using MicroPlate Manager Software (BioRad). 20 X sample buffer (100 % β-
581 mercaptoethanol, and bromophenol blue) was added to lysates and were subsequently incubated
582 for an additional 5 minutes. Lysates were separated using Mini-PROTEAN TGX 4 to 15% gradient
583 gels (25 mM tris, 192 mM glycine, and 0.1% (w/v) SDS; Bio-Rad, 4561086) and transferred at 4°C
584 to either Immobilon-FL or Immunoblon-P (IPVH00010) polyvinylidene fluoride membranes (Merck,
585 IPFL00010) (1.5 hours; 250 mA, 25 mM tris, 192 mM glycine, and 5% (v/v) methanol).
586 Immobilon-FL membranes were dried for 1 hour at room temperature, washed in ultrapure water,
587 100% methanol, Tris buffered saline (TBS) in the listed order and blocked using Odyssey blocking
588 buffer (Li-COR, 927-40000). They were then incubated in primary antibodies (supplementary table
589 7) diluted in Odyssey blocking buffer supplemented with 0.2% (v/v) Tween 20 (Sigma-Aldrich,
590 P9416) overnight at 4°C, washed three times with TBS containing 0.1% (v/v) Tween 20 and
591 incubated with IRDye-conjugated secondary antibodies (supplementary table 7) diluted in Odyssey
592 blocking buffer supplemented with 0.2% (v/v) Tween 20 and 10% (v/v) sodium dodecyl sulfate (SDS)
593 for 1 hour at room temperature. Immobilon-FL membranes were washed in PBS and protein was
594 visualised and quantified using the Odyssey CLx and Image Studio Lite software 2 (Li-COR).
595 Immunoblon-P membranes were blocked in TBS supplemented with 5% (w/v) skim milk powder and
596 Tween 20, incubated with primary antibodies (supplementary table 7) diluted in the same solution at
597 4°C overnight, washed three times with TBS containing 0.1% (v/v) Tween 20 and incubated with
598 horseradish peroxidase-conjugated secondary antibodies (supplementary table 7) at room
599 temperature for 1 hour. Protein was subsequently visualised using Amersham ECL Plus (GE
600 Healthcare, RPN2132) and Super RX film (Fujifilm, 03G01).
601
602 Total RNA-sequencing
603 Cells (1e+06^6 per treatment condition) were centrifuged (1400rpm at 4°C for 4 minutes), washed in
604 ice-cold PBS and resuspended in 350µl of Buffer RLT Plus supplemented with 1% (v/v) β-
605 mercaptoethanol from the RNeasy Plus Mini Kit (Qiagen, 74134). RNA was extracted using the same
606 kit according to manufacturer's instructions and quality was assessed using the Agilent 2200
607 TapeStation System (Agilent, G2964AA) with RNA ScreenTape (Agilent, 5067-5576) and Sample

608 Buffer (Agilent, 5067-5577). S2 spike-in material (5%) was added to RNA. Sequencing libraries were
609 prepared using NEBNext Ultra II Directional RNA Library Prep Kit for Illumina, where ribodepletion
610 was performed using the NEBNext rRNA Depletion Kit (New England BioLabs, E6310). Paired-end
611 75 base pair (bp) reads were sequenced using the NextSeq 500 (Illumina).
612
613 3'UTR-sequencing
614 Cells were treated with DMSO or AZ-5576 (CDK9i; 100nM) for 6 hours at 37°C and 5% carbon
615 dioxide. Following incubation, cells were harvested, centrifuged (500g at 4°C for 4 minutes), washed
616 in ice-cold PBS and resuspended in 600µL TRIzol. RNA was extracted using the Directzol RNA
617 Miniprep Kit, where an additional DNase I digestion step was performed (Zymogen; R2052).
618 Sequencing libraries were prepared using the QuantSeq 3′mRNA-seq Library Prep Kit FWD for
619 Illumina (Lexogen, Vienna, Austria) and sequenced as single-end 75 base pair reads using the
620 NextSeq 500 (Illumina).
621
622 SLAM-sequencing
623 Protocol was adapted from (*18*). K562 and THP-1 cells (1e+06 per treatment) were first pre-treated
624 with small molecule inhibitors for a total time of 2 hours to pre-establish protein-target inhibition.
625 Newly synthesized RNA in K562 cells was then labelled using 100 µM 4-sU in the final 1 hour of
626 treatment at 37°C and 5% carbon dioxide. Cells were washed in ice-cold PBS and resuspended in
627 300µL TRIzol. For direct measurement of RNA half-lives, newly synthesized RNA was labelled by
628 incubating cells in 30µM 4-sU for 12 hours at 37°C and 5% carbon dioxide, whereby culture medium
629 was exchanged every 3 hours for the duration of the pulse. For the uridine chase, cells were
630 centrifuged (1400rpm at 4°C for 4 minutes), washed in sterile ice-cold PBS twice and resuspended
631 in pre-warmed (37°C) culture medium containing 3mM uridine (Sigma Aldrich, U6381). At 0- ,1-, 2-,
632 4-, 8-, 12- hours for K562 cells and 0-, 0.3-, 0.6-, 1-, 2-. 4-, 8- hours for THP-1 cells post the uridine
633 chase, cells were harvested, centrifuged (1400rpm at 4°C for 4 minutes) and resuspended in 300µL
634 TRIzol. For treatment-specific RNA decay rates, cells were centrifuged (1400rpm at 4°C for 4
635 minutes), washed in sterile ice-cold PBS twice and resuspended in pre-warmed (37°C) culture
636 medium containing 3mM uridine (Sigma Aldrich, U6381) and either 1µM DMSO, JQ1 or AZ-5576. At
637 0-, 2-, 4- and 8- hours post uridine chase/drug addition, cells for each treatment condition were
638 harvested, centrifuged (1400rpm at 4°C for 4 minutes) and resuspended in 300µL TRIzol. All SLAM-
639 seq experiments included a non- 4-sU labelled control unless otherwise stated. To extract RNA, one-
640 fifth volume of chloroform was added to TRIzol lysates, followed by shaking, incubation at room
641 temperature for 2 minutes and centrifugation (16000g at 4°C for 15 minutes). The aqueous phase
642 was isolated and RNA was precipitated using DTT (10mM), 100% isopropanol (1 volume) and
643 GlycolBlue co-precipitant (15ug, Ambion, AM9515), incubated at room temperature for 10 minutes
644 and centrifuged (16000g at 4°C for 20 minutes). Supernatant was removed, RNA pellets were
645 washed in 75% (v/v) ethanol and DTT (100µM) and centrifuged (7500g at room temperature for 5
646 minutes). Supernatant was removed and RNA pellets dried for 10 minutes prior to reconstitution in
647 Ultrapure DNAse/RNAse-free distilled water (Thermo Fisher Scientific, 10977023) supplemented
648 with DTT (1mM) and incubation at 55°C for 10 minutes. Thiol-containing bases were reduced by
649 incubating RNA (10µg) with IAA (10mM, 50 mM $NaPO_4$ pH 8.05 and 50% (v/v) DMSO) in a final
650 volume of 50µL for 15 minutes at 55°C. Reaction was stopped by quenching IAA with DTT (20µM).
651 RNA was precipitated using 3M NaOAc pH 5.2 (5µL), 100% ethanol (125µL) and GlycolBlue co-
652 precipitant, incubated at -80°C for 30 minutes and centrifuged (16000g at 4°C for 30 minutes).
653 Supernatant was removed and RNA pellet was washed in 75% (v/v) ethanol and centrifuged (16000g
654 at 4°C for 10 minutes) twice, dried at room temperature for 10 minutes and reconstituted in Ultrapure
655 DNAse/RNAse-free distilled water. RNA clean-up was performed by incubating RNA solution in 2
656 volumes of AMPure XP Beads (Beckman Coulter, A63881) for 2 minutes at room temperature.
657 Beads were washed in 80% (v/v) ethanol twice, dried at room temperature for 3 minutes and
658 resuspended in Ultrapure DNAse/RNAse-free distilled water. Eluate was collected and RNA quality

659 and concentration was assessed using the Agilent 2200 TapeStation System (Agilent, G2964AA)
660 with RNA ScreenTape (Agilent, 5067-5576) and Sample Buffer (Agilent, 5067-5577). S2 spike-in
661 material (5%) was added to RNA. Sequencing libraries were prepared using the QuantSeq 3′mRNA-
662 seq Library Prep Kit FWD for Illumina (Lexogen, Vienna, Austria) and sequenced as single-end 75
663 base pair reads using the NextSeq 500 (Illumina).
664
665 TT-sequencing
666 Protocol is adapted from (*21*). Cells (5e+07 per treatment condition) were incubated with 1mM 4sU
667 for either 5 or 15 minutes at 37°C and 5% carbon dioxide, centrifuged (1400rpm at 4°C for 5 minutes)
668 and resuspended in TRIzol (5mL). One-fifth volume of chloroform was added to lysates, followed by
669 shaking, incubation at room temperature for 2 minutes and centrifugation (13000g at 4°C for 10
670 minutes). The aqueous phase was isolated and RNA was precipitated using 100% isopropanol (1
671 volume), incubated at room temperature for 10 minutes and centrifuged (13000rpm at 4°C for 10
672 minutes). Supernatant was removed and RNA pellet was washed in 70% (v/v) ethanol, reconstituted
673 in Ultrapure DNAse/RNAse-free distilled water (100µL) and denatured at 65°C for 10 minutes. S2
674 spike-in (15µg) was added to RNA (150µg), material was adjusted to a final volume 100µL and
675 sonicated in microTUBE AFA Fiber screw cap tubes (6 mm × 16 mm, Covaris, 520096) using the
676 Covaris S220 Focused-ultrasonicator at a maximum power for 15 seconds. Thiol-specific
677 biotinylation of RNA was performed in a final volume of 1.5mL by incubation with 10 mM tris (pH
678 7.4), 1 mM EDTA, 20% (v/v) dimethylformamide (200 µg/ml; Sigma-Aldrich, 227056), and 300 µg of
679 EZ-Link HPDP-Biotin (Thermo Fisher Scientific, 21341) for 1.5 hours at room temperature. An equal
680 volume of chloroform was added to reaction, followed by shaking, incubation at room temperature
681 for 2 minutes and centrifugation (1400rpm at 4°C for 5 minutes). Aqueous phase was isolated and
682 an equal volume of chloroform was added, followed by shaking, incubation at room temperature for
683 2 minutes and centrifugation (1400rpm at 4°C for 5 minutes). This step was repeated an additional
684 one time. Aqueous phase was isolated and RNA was precipitated using 5M NaCl (10% volume) and
685 100% isopropanol (1 volume) and centrifugation (20000g at 4°C for 20 minutes). RNA pellets were
686 washed in 75% (v/v) ethanol, reconstituted in Ultrapure DNAse/RNAse-free distilled water (100µL)
687 and denatured at 65°C for 10 minutes. Biotinylated RNA was separated from the total RNA pool by
688 incubation with streptavidin beads (µMACs Streptavidin Kit, Miltenyi Biotec, Bergisch Gladbach,
689 Germany, 130-074-101) at room temperature for 15 min with constant rotation. µMACs columns pre-
690 equilibrated with room temperature wash buffer (100 mM tris-HCl (pH 7.4), 10 mM EDTA, 1 M NaCl,
691 and 0.1% (v/v) Tween 20) were used to bind streptavidin beads, which were then washed using
692 900µL wash buffer that was heated to 65 °C or at room temperature, 5 times each. Biotinylated RNA
693 was eluted into 700µL Buffer RLT from the RNeasy MinElute Cleanup Kit (Qiagen, 74204) through
694 two additions of 100 mM DTT (100µl) 3 min apart, and then isolated using the same kit according to
695 manufacturer's instructions. RNA concentration was quantified using the Agilent 2200 TapeStation
696 System (Agilent, G2964AA) with High Sensitivity RNA ScreenTape (Agilent, 5067-5579) and Sample
697 Buffer (Agilent, 5067-5580).
698 Sequencing libraries were prepared with the NEBNext Ultra II Directional RNA Library Prep Kit for
699 Illumina (without additional fragmentation), where ribodepletion was performed using the NEBNext
700 rRNA Depletion Kit (New England BioLabs, E6310). Single-end 75 base pair reads were sequenced
701 using the NextSeq 500 (Illumina).
702
703 MAC-seq
704 Cells (5e+04 per well) in a final volume of 100µL in a 96-well plate format were incubated with
705 transcriptional and epigenetic inhibitors in technical duplicate for 6 hours (supplementary table 8) at
706 37°C and 5% carbon dioxide. 5e+03 cells from each well were aliquoted into a separate 96-well
707 plate, washed in ice-cold PBS twice and centrifuged (1400rpm at 4°C for 4minutes). Supernatant
708 was removed and cell pellets were frozen at -80°C. Library preparation is adapted from (*61*). In detail,
709 17 µl lysis buffer were added into each well of a 96-well plate containing cell pellets and incubated

710 at room temperature for 15 min under agitation (900 rpm). 12.5 µl of cell lysate were transferred into
711 each well of a new 96-well plate previously prepared with 1 µl of 10 nM well-specific RT MAC-seq
712 primer and 7.5 µl RT mix; the RT mix contains a TSO primer and external ERCC RNAs. The mixture
713 was incubated for 2 hours at 42 C to create well-barcoded full length cDNA and then all the wells of
714 a plate were combined into a single tube. Concentration and clean-up was done via column
715 purification (DNA Clean and Concentrator™-100, Zymo Research) and RNAClean XP beads
716 (Beckman Coulter) and each plate eluted in 22 µl nuclease free water. The purified cDNA was pre-
717 amplified with KAPA HiFi HotStart ReadyMix (Roche) and MAC-seq PreAmp PCR primer and the
718 quality checked on a D5000 Screentape (TapeStation, Agilent). One barcoded library was prepared
719 per plate using TD buffer and TDE1 enzyme (Illumina) for tagmentation and KAPA HiFi HotStart
720 Ready Mix (Roche) and custom primers (MAC-seq P5 PCR and MAC-seq Indexing Mix) for
721 amplification. Libraries were purified with DNA Ampure XP beads (Beckman Coulter), quality
722 checked on a DNA1000 tape (TapeStation, Agilent) and quantity verified by qPCR. Two indexed
723 libraries were sequenced on a NextSeq 500 instrument (Illumina) using a custom sequencing primer
724 (MAC-seq Read primer) and a High Output Kit v2.5 75 Cycles (Illumina) with paired-end
725 configuration (25 base pairs for read 1 and 50 base pairs for read 2).
726
727 SLAM-seq analysis
728 Single-end reads were demultiplexed using bcl2fastq (v2.17.1.14) and resulting FASTQ files were
729 trimmed for adapter sequences using Trim_galore (v0.6.5) with a stringency overlap of 3bp. Trimmed
730 FASTQ files were processed with SLAM-dunk (v0.4.3), enabling multi-mapper reconciliation and
731 using a threshold of at least 2 T > C conversions to mark a read as converted. The no 4sU control
732 sample was processed first to find single nucleotide polymorphisms (SNPs), which was then used
733 to filter the subsequent samples. `bedtools merge` was then used to merge the 3' UTRs of each
734 Ensembl transcript by gene (v77 identifiers for hg38) for use in the SLAM-dunk counting step. The
735 Broad Institute GSEA software was used to perform GSEA (*62*). Differential gene testing was
736 performed on counts normalized to library sizes scaled to external S2 spike-ins and filtered for lowly
737 expressed genes using edgeR (v3.32.1) on Rstudio (v4.0.2). SLAM sequencing tcount files from (*30*)
738 (GEO accession GSE138210) and (*11*) (GEO accession GSE111463) were downloaded and
739 differential gene testing was performed as described above.
740
741 TT-seq analysis
742 Single-end reads were demultiplexed using bcl2fastq (v2.17.1.14) and resulting FASTQ files were
743 aligned to the genome using STAR (v2.7), which were then summarized using featureCounts in
744 Subread (v2.0.1): counting reads with a minimum Mapping Quality Score (MQS) of 7 in the union of
745 all transcript isoforms of each Ensembl gene. Only genes with at least 10 reads per million across at
746 least two samples within an experiment were retained for further analysis. In order to compare
747 expression levels between samples, raw read counts for each gene were converted to reads per
748 million using adjusted library sizes calculated with edgeR's TMM implementation on the spike-in read
749 counts.
750
751 Total RNA-seq analysis
752 Paired-end reads were demultiplexed using bcl2fastq (v2.17.1.14) and resulting FASTQ files were
753 quality checked using fastqc (v0.11.6), trimmed 15 bp from the 5' end to remove primer bias and
754 filtered for quality and length using cutadapt (v2.1; -u 15 -U 15 -q 15 --pair-filter any --minimum-
755 length 50). Trimmed reads were mapped to GRCh38/hg38 and BDGP6/dm6 genomes using hisat2
756 (v2.1.0) with paired read settings and resulting SAM files were converted to BAM files using samtools
757 (v1.9; view), which were then sorted and indexed. Reads mapping to either exonic or intronic
758 genomic intervals were counted using a combined hg38/dm6/GFP GTF file with FeatureCounts from
759 the subread package (v2.0.0; featureCounts -O -M -T 32 -p -s 2). Differential gene testing was
760 performed on counts normalized to library sizes scaled to external S2 spike-ins and filtered for lowly

761 expressed genes using edgeR (v3.32.1) on Rstudio (v4.0.2). Gene Ontology analysis was performed
762 using the ToppGene suite (*63–65*).
763
764 3'UTR-seq analysis
765 Single-end reads were demultiplexed using bcl2fastq (v2.17.1.14) and resulting FASTQ files were
766 quality checked using fastqc (v0.11.6), trimmed 12 bp from the 5' end to remove primer bias, trimmed
767 for polyA stretches, and filtered for quality and length using cutadapt (v2.1; -u 12 -q 10 -m 20 -a
768 AAAAAAAAAA). Trimmed reads were mapped to GRCh37/hg19 and BDGP R5/dm3 genomes using
769 hisat2 (v2.1.0) using standard single-end settings and resulting SAM files were converted to BAM
770 files using samtools (v1.9; view), which were then sorted (sort) and indexed (index). Reads mapping
771 to exonic genomic intervals were counted using a hg19 GTF file and dm3 SAF file with
772 FeatureCounts from the subread package (v2.0.0; featureCounts -O -M -F GTF -T 16 -s 0).
773 Differential gene testing was performed on counts normalized to library sizes scaled to external S2
774 spike-ins and filtered for lowly expressed genes using edgeR (v3.32.1) on Rstudio (v4.0.2). The
775 Broad Institute GSEA software was used to perform GSEA (*62*).
776
777 MAC-seq analysis
778 Paired-end reads were demultiplexed using bcl2fastq (v2.17.1.14) and resulting FASTQ files were
779 quality checked using fastqc (v0.11.6) and read 2 (R2) was trimmed 15 bp from the 5' end to remove
780 primer bias using cutadapt (v2.1; -u 15). R2 FASTQ files of paired-end reads were demultiplexed
781 according to well barcodes (supplementary table 9) and filtered for PCR duplicates using Unique
782 Molecular Identifiers (UMIs), both present in read 1 (R1) using the scruff (*66*) R (v4.0.2) package
783 dumultiplex function (bcStart = 1, bcStop = 10, bcEdit = 0, umiStart = 11, umiStop = 20, keep = 35,
784 minQual = 20, yieldReads = 1e+06). R2 FASTQ files were then mapped to the GRCh37/hg19
785 genome and ERCC sequences using alignRsubread (unique = FALSE, nBestLocations = 1, format
786 = "BAM") and resulting BAM files were used to count unique R2 reads mapping to exonic genomic
787 intervals and ERCC sequences using a combined hg19/ERCC GTF file with countUMI (umiEdit = 0,
788 format = "BAM", cellPerWell = 1. Both functions are from the scruff R package. Gene expression
789 counts were normalized to library size and reads mapping to ERCC spike-ins using the RUVseq R
790 package (v1.24.1). Subsequent count processing was performed using the Seurat R package
791 (v3.2.1) (*67*), where lowly expressed genes were filtered and counts were normalized for latent
792 variables including plate, well row and column, using the SCTransform function. SCTransformed
793 scaled gene RNA expression values were then used for PCA, where shared-nearest-neighbours
794 (SNN) network was calculated using the top 10 Principal Components with the FindNeighbours
795 function using default parameters. Drug-treatment clusters were subsequently identified with the
796 Louvain algorithm using a resolution parameter of 2. Uniform Manifold Approximation and Projection
797 (UMAP) values were also calculated using the top 10 Principal Components with the RunUMAP
798 function using default parameters. Differential gene testing relative to treatment controls (DMSO or
799 EtOH) was performed using a hurdle model (MAST) with un-scaled gene RNA expression counts,
800 plate and column numbers as latent variables and a logFC threshold of 0 with the FindMarkers
801 Function. Area Under the Curve (AUC) scores for each drug treatment and gene lists indicated was
802 calculated using all expressed genes with the R AUCell Package (v0.10.0).
803
804 ChIP-seq analysis and super-enhancer identification
805 H3K27ac ChIP-seq FASTQ files (SRR1957037, SRR1957038, GEO Accession GSM1652918) were
806 downloaded using sratoolkit (v2.9.0, fastq-dump --gzip --split-files), quality checked using fastqc
807 (v0.11.6) and mapped to the GRCh37/hg19 genome using bowtie2 (v2.3.4.1) with paired end read
808 settings. Resulting SAM files were converted to BAM files using samtools (v1.9; view), which were
809 then sorted and indexed. Potential PCR duplicates were filtered using the MarkDuplicates function
810 from picard (v2.6.0; REMOVE_DUPLICATES= true) and BAM files were converted to TDF files using
811 igvtools (v2.3.95; count -z 5 -w 10). H3K27ac peaks were called relative to input using macs (v2.1.1;

812 callpeak -f BAMPE -g hs -q 0.01 -call-summits –cutoff-analysis) and peaks within hg19 ENCODE
813 blacklist regions (https://www.encodeproject.org/files/ENCFF356LFX/) were removed using
814 bedtools (v2.27.1) intersect function. Super-enhancer calling was performed using Ranking Ordering
815 of Super-Enhancer (ROSE2) (v1.0.5; -c INPUT -g hg19 -t 2000 -s 12500) (*68*) and were annotated
816 to genes according to "TOP GENE."
817
818 Genome-wide CRISPR Cas9 screening analysis
819 Trimmed 20 base pair reads from survival screens performed in THP-1 and MV4;11 Cas9 cells
820 transduced with the Brunello genome-wide sgRNA library and cultured in either DMSO or AZ-5576
821 (CDK9i; 150nM) for 21 days from (*69*), were used for sgRNA counting with the MAGeCK algorithm,
822 where read counts from treatment replicates were pooled (v0.5.6; mageck count). The MAGeCK
823 algorithm test subcommand (mageck test) was then used to determine genes negatively selected in
824 CDK9i relative to DMSO treatment groups. Visualization of screen data was performed in R (v4.0.2)
825 using ggplot2 (v3.1.1) and ggrepel (v0.8.1) packages. Annotated RBPs were identified using data
826 from (*70*).
827
828 Coltron analysis
829 The coltron algorithm (v1.0.2) (*27*) was used to identify SE-associated TFs and regulatory networks
830 using ROSE2-determined super-enhancer peaks and H3K27ac BAM signal with default parameters.
831
832 TCGA survival analysis
833 SEM (RNA-Seq by Expectation Maximization) (*71*) scaled expression values (transcripts per million)
834 for TCGA tumour samples were downloaded from the GDAC Firehose website. Entrez gene IDs
835 were mapped to HGNC gene symbols using the biomaRt R package (version 2.42.0) and collapsed
836 to unique values per gene symbol by selecting the most variable entrez ID among all samples for
837 each gene symbol. Primary samples from the TCGA LAML cohort were selected using the
838 TCGA biolinks R package (version 2.14.0) and were matched with overall survival (OS) endpoints
839 from the TCGA Pan-Cancer Clinical Data Resource. Gene signature scores were calculated using
840 the singscore R package,then used to fit Kaplan-Meier and Cox regression models to the OS
841 endpoints using the survival R package (version 3.1-8).
842
843 Determination of RNA synthesis and decay rates
844 Solving the first order differential equation in Fig. 2F yields an exponential function with parameters
845 for the synthesis rate (k_1), decay rate (k_2) and initial quantity of RNA (M_0):
846 $M(t) = (M_0 - K) * e^{(-k_2*t)} + K$
847 where $K = k_1/k_2$ is the quantity at equilibrium.
848 To determine decay rates (k_2) for each gene, precision-weighted nonlinear regression was used to
849 fit an exponential curve to the decreasing quantity of SLAM-seq labelled reads measured post-
850 washout of 4sU.
851 Assuming no synthesis of labelled reads post-washout ($k_1 = 0$) leaves one parameter for the starting
852 RNA concentration, which was set to the initial data point at T = 0, and one for the decay rate, which
853 was fit using MINPACK's (v1.2-1) Levenberg-Marquardt implementation in R.
854 Precision weights for the fit were estimated using local regression. The standard deviation between
855 technical replicates for a given mean expression level in the baseline SLAM-seq dataset was
856 modelled with R's `loess` implementation, and then applied to calculate weights for the other
857 samples during fitting.
858 Synthesis rates were determined by dividing the TT-seq adjusted reads per million for each gene by
859 the length and sampling time, producing a scaled FPKM h^{-1} averaged across replicates.
860
861 Predictions

Predictions were made with the model using the fitted rates and differing initial conditions, then compared against a separate dataset of total mRNA measurements at T = 2, 6h.

Parameters set for simulated results:

Simulated Result	**Decay rate (k_1)**	**Synth. rate (k_2)**	**Initial qty (M_0)**
Simulated total transcriptional shutdown	Fitted decay rate under drug	0	Baseline equilibrium

Acknowledgments

We thank members of the Victorian Centre for Functional Genomics, Peter MacCallum Centre Molecular Genomics Core, Daniel Ho from Novartis and the other authors for their help during DRUG-seq protocol implementation and Compounds Australia at Griffith University for their provision of specialized compound management and logistics research services to the project.

Funding

I.T. was supported by an Australian Government Research Training Scholarship. S.J.V. was supported by a Rubicon fellowship (NWO, 019.161LW.017), NHMRC EL1 fellowship (GNT1178339), and The Kids' Cancer Project. R.W.J was supported by the Cancer Council Victoria, National Health and Medical Research Council of Australia (NHMRC), and The Kids' Cancer Project. A.T.P. was supported by a National Health and Medical Research Council (NHMRC) Senior Research Fellowship (1116955). B.F. and A.T.P. were supported by the Lorenzo and Pamela Galli Charitable Trust and the Galli Next Generation Discoveries Initiative. The Victorian Centre for Functional Genomics (K.J.S.) is supported by the Australian Cancer Research Foundation (ACRF). G.M.A. is supported by a PeterMac Foundation Grant (ID # 1739), Phenomics Australia (PA) through funding from the Australian Government's National Collaborative Research Infrastructure Strategy (NCRIS) program, the Peter MacCallum Cancer Centre Foundation and the University of Melbourne Research Collaborative Infrastructure Program (MCRIP). Equipment used for this work was funded by the (Australian Cancer Research Foundation (ACRF, Tumour Heterogeneity Program). The research benefitted by support from the Victorian State Government Operational Infrastructure Support and Australian Government NHMRC Independent Research Institute Infrastructure Support.

Author contributions

I.T. performed experiments, next generation sequencing analysis, data interpretation and wrote the manuscript. B.F. and A.T.P performed next generation sequencing analysis and computational modelling. Z.F. designed sgRNA and plasmid templates for CRISPR-HDR. S.G., D.Y., G.M.A. and K.J.S. optimized and performed DRUG-seq. I.Y.K. performed Myc intracellular staining and total cell number assays and analysis and was supervised by E.D.H. S.B. performed combination therapy experiments. M.Z. performed TCGA analysis. S.J.V. and R.W.J. performed data interpretation, study supervision and co-wrote the manuscript. All co-authors proof-read and edited the manuscript.

Competing interests:

The Johnstone laboratory receives funding support from Roche, BMS, Astra-Zeneca and MecRx. RWJ is a shareholder and consultant for MecRx.

905 ***References***

906 1. J. E. Bradner, D. Hnisz, R. A. Young, Transcriptional Addiction in Cancer. *Cell*. **168**,
907 629–643 (2017).
908 2. M. J. Bywater, R. B. Pearson, G. A. Mcarthur, R. D. Hannan, Dysregulation of the
909 basal RNA polymerase transcription apparatus in cancer. *Nat. Rev. Cancer*. **13**
910 (2013), doi:10.1038/nrc3496.
911 3. E. Smith, C. Lin, A. Shilatifard, The super elongation complex (SEC) and MLL in
912 development and disease. *Genes Dev.* **25**, 661–672 (2011).
913 4. C. Villicaña, G. Cruz, M. Zurita, The basal transcription machinery as a target for
914 cancer therapy (2014).
915 5. N. Laham-karam, G. P. Pinto, A. Poso, P. Kokkonen, Transcription and Translation
916 Inhibitors in Cancer Treatment. **8**, 1–24 (2020).
917 6. S. M. Abedin, C. S. Boddy, H. G. Munshi, BET inhibitors in the treatment of
918 hematologic malignancies: Current insights and future prospects. *Onco. Targets.*
919 *Ther.* (2016), , doi:10.2147/OTT.S100515.
920 7. G. E. Winter, D. L. Buckley, J. Paulk, J. M. Roberts, A. Souza, S. Dhe-paganon, J. E.
921 Bradner, Phthalimide conjugation as a strategy for in vivo target protein degradation.
922 *Science (80-.).* **348**, 1376–1382 (2015).
923 8. L. M. Lasko, C. G. Jakob, P. Rohinton, W. Qiu, D. Montgomery, E. L. Digiammarino,
924 T. M. Hansen, R. M. Risi, R. Frey, V. Manaves, B. Shaw, M. Algire, P. Hessler, L. T.
925 Lam, T. Uziel, E. Faivre, D. Ferguson, F. G. Buchanan, R. L. Martin, M. Torrent, G. G.
926 Chiang, K. Karukurichi, J. W. Langston, B. T. Weinert, C. Choudhary, P. De Vries, A.
927 F. Kluge, M. A. Patane, J. H. Van Drie, C. Wang, D. Mcelligott, E. A. Kesicki, R.
928 Marmorstein, C. Sun, P. A. Cole, S. H. Rosenberg, M. R. Michaelides, A. Lai, K. D.
929 Bromberg, Discovery of a selective catalytic p300/CBP inhibitor that targets lineage-
930 specific tumours. *Nature*. **550**, 128–132 (2017).
931 9. O. Bensaude, Inhibiting eukaryotic transcription: Which compound to choose? How to
932 evaluate its activity? *Transcription*. **2**, 103–108 (2011).
933 10. R. D. Martin, T. E. Hébert, J. C. Tanny, Therapeutic targeting of the general RNA
934 polymerase II transcription machinery. *Int. J. Mol. Sci.* **21** (2020),
935 doi:10.3390/ijms21093354.
936 11. M. Muhar, A. Ebert, T. Neumann, C. Umkehrer, J. Jude, C. Wieshofer, P.
937 Rescheneder, J. J. Lipp, V. A. Herzog, B. Reichholf, D. A. Cisneros, T. Hoffmann, M.
938 F. Schlapansky, P. Bhat, A. Von Haeseler, T. Köcher, A. C. Obenauf, J. Popow, S. L.
939 Ameres, J. Zuber, SLAM-seq defines direct gene-regulatory functions of the BRD4-
940 MYC axis. *Science (80-.).* **360**, 800–805 (2018).
941 12. C. Neumayr, V. Haberle, L. Serebreni, K. Karner, O. Hendy, A. Boija, J. E. Henninger,
942 C. H. Li, K. Stejskal, G. Lin, K. Bergauer, M. Pagani, M. Rath, K. Mechtler, C. D.
943 Arnold, A. Stark, Differential cofactor dependencies define distinct types of human
944 enhancers. *Nature*. **606**, 406–413 (2022).
945 13. J. Zuber, J. Shi, E. Wang, A. R. Rappaport, H. Herrmann, E. A. Sison, D. Magoon, J.
946 Qi, K. Blatt, M. Wunderlich, M. J. Taylor, C. Johns, A. Chicas, J. C. Mulloy, S. C.
947 Kogan, P. Brown, P. Valent, J. E. Bradner, S. W. Lowe, C. R. Vakoc, RNAi screen
948 identifies Brd4 as a therapeutic target in acute myeloid leukaemia. *Nature*. **478**, 524–
949 528 (2011).
950 14. J. E. Delmore, G. C. Issa, M. E. Lemieux, P. B. Rahl, J. Shi, H. M. Jacobs, E.
951 Kastritis, T. Gilpatrick, R. M. Paranal, J. Qi, M. Chesi, A. C. Schinzel, M. R. McKeown,
952 T. P. Heffernan, C. R. Vakoc, P. L. Bergsagel, I. M. Ghobrial, P. G. Richardson, R. A.
953 Young, W. C. Hahn, K. C. Anderson, A. L. Kung, J. E. Bradner, C. S. Mitsiades, BET
954 bromodomain inhibition as a therapeutic strategy to target c-Myc. *Cell*. **146**, 904–917
955 (2011).
956 15. M. A. Dawson, R. K. Prinjha, A. Dittmann, G. Giotopoulos, M. Bantscheff, W. Chan, S.
957 C. Robson, C. Chung, C. Hopf, M. M. Savitski, C. Huthmacher, E. Gudgin, D. Lugo, S.
958 Beinke, T. D. Chapman, E. J. Roberts, P. E. Soden, K. R. Auger, O. Mirguet, K.
959 Doehner, R. Delwel, A. K. Burnett, P. Jeffrey, G. Drewes, K. Lee, B. J. P. Huntly, T.
960 Kouzarides, Inhibition of BET recruitment to chromatin as an effective treatment for
961 MLL-fusion leukaemia. *Nature*. **478**, 529–533 (2011).
962 16. J. Shi, W. A. Whyte, C. J. Zepeda-Mendoza, J. P. Milazzo, C. Shen, J. S. Roe, J. L.
963 Minder, F. Mercan, E. Wang, M. A. Eckersley-Maslin, A. E. Campbell, S. Kawaoka, S.

964 Shareef, Z. Zhu, J. Kendall, M. Muhar, C. Haslinger, M. Yu, R. G. Roeder, M. H.
965 Wigler, G. A. Blobel, J. Zuber, D. L. Spector, R. A. Young, C. R. Vakoc, Role of
966 SWI/SNF in acute leukemia maintenance and enhancer-mediated Myc regulation.
967 *Genes Dev.* **27**, 2648–2662 (2013).
968 17. J. S. Roe, F. Mercan, K. Rivera, D. J. Pappin, C. R. Vakoc, BET Bromodomain
969 Inhibition Suppresses the Function of Hematopoietic Transcription Factors in Acute
970 Myeloid Leukemia. *Mol. Cell*. **58**, 1028–1039 (2015).
971 18. V. A. Herzog, B. Reichholf, T. Neumann, P. Rescheneder, P. Bhat, T. R. Burkard, W.
972 Wlotzka, A. Von Haeseler, J. Zuber, S. L. Ameres, Thiol-linked alkylation of RNA to
973 assess expression dynamics. *Nat. Methods*. **14**, 1198–1204 (2017).
974 19. A. Lusser, C. Gasser, L. Trixl, P. Piatti, I. Delazer, D. Rieder, J. Bashin, C. Riml, T.
975 Amort, R. Micura, Thiouridine-to-Cytidine Conversion Sequencing (TUC-Seq) to
976 Measure mRNA Transcription and Degradation Rates. *Methods Mol. Biol.* (2020),
977 doi:10.1007/978-1-4939-9822-7_10.
978 20. J. A. Schofield, E. E. Duffy, L. Kiefer, M. C. Sullivan, M. D. Simon, TimeLapse-seq:
979 Adding a temporal dimension to RNA sequencing through nucleoside recoding. *Nat.*
980 *Methods*. **15**, 221–225 (2018).
981 21. M. Michel, B. Zacher, C. Demel, A. Tresch, J. Gagneur, TT-seq maps the human
982 transient transcriptome. *Science (80-.).* **352** (2016).
983 22. M. Rabani, J. Z. Levin, L. Fan, X. Adiconis, R. Raychowdhury, M. Garber, A. Gnirke,
984 C. Nusbaum, N. Hacohen, N. Friedman, I. Amit, A. Regev, Metabolic labeling of RNA
985 uncovers principles of RNA production and degradation dynamics in mammalian cells.
986 *Nat. Biotechnol.* **29** (2011), doi:10.1038/nbt.1861.
987 23. E. E. Duffy, D. Catherine, R. R. Kitchen, B. Mark, M. D. Simon, E. E. Duffy, M.
988 Rutenberg-schoenberg, C. D. Stark, R. R. Kitchen, M. B. Gerstein, M. D. Simon,
989 Tracking Distinct RNA Populations Using Efficient and Reversible Covalent Chemistry
990 Technology Tracking Distinct RNA Populations Using Efficient and Reversible
991 Covalent Chemistry. *Mol. Cell*. **59**, 858–866 (2015).
992 24. J. A. Mertz, A. R. Conery, B. M. Bryant, P. Sandy, S. Balasubramanian, D. A. Mele, L.
993 Bergeron, R. J. Sims, Targeting MYC dependence in cancer by inhibiting BET
994 bromodomains. *Proc. Natl. Acad. Sci. U. S. A.* **108**, 16669–16674 (2011).
995 25. P. K. Parua, G. T. Booth, M. Sansó, B. Benjamin, J. C. Tanny, J. T. Lis, R. P. Fisher,
996 A Cdk9-PP1 switch regulates the elongation-termination transition of RNA polymerase
997 II. *Nature*. **558**, 460–464 (2018).
998 26. Q. Jia, S. Chen, Y. Tan, Y. Li, F. Tang, Oncogenic super-enhancer formation in
999 tumorigenesis and its molecular mechanisms. *Exp. Mol. Med.* **52**, 713–723 (2020).
1000 27. C. J. O. Alexander J. Federation, Donald R. Polaski, A. Fan, C. Y. Lin, J. E., Bradner,
1001 Identification of candidate master transcription factors within enhancer-centric
1002 transcriptional regulatory networks. *bioRxiv* (2018).
1003 28. T. Yamada, N. Akimitsu, Contributions of regulated transcription and mRNA decay to
1004 the dynamics of gene expression. *Wiley*, 1–18 (2019).
1005 29. Q. Wu, S. G. Medina, G. Kushawah, M. L. Devore, L. A. Castellano, J. M. Hand, M.
1006 Wright, A. A. Bazzini, Translation affects mRNA stability in a codon-dependent
1007 manner in human cells. *Elife*, 1–22 (2019).
1008 30. O. Gilan, I. Rioja, K. Knezevic, M. J. Bell, M. M. Yeung, N. R. Harker, E. Y. N. Lam, C.
1009 Chung, P. Bamborough, M. Petretich, M. Urh, S. J. Atkinson, A. K. Bassil, E. J.
1010 Roberts, D. Vassiliadis, M. L. Burr, A. G. S. Preston, C. Wellaway, T. Werner, J. R.
1011 Gray, A. M. Michon, T. Gobbetti, V. Kumar, P. E. Soden, A. Haynes, J. Vappiani, D. F.
1012 Tough, S. Taylor, S. J. Dawson, M. Bantscheff, M. Lindon, G. Drewes, E. H. Demont,
1013 D. L. Daniels, P. Grandi, R. K. Prinjha, M. A. Dawson, Selective targeting of BD1 and
1014 BD2 of the BET proteins in cancer and immunoinflammation. *Science (80-.).* **368**,
1015 387–394 (2020).
1016 31. A. Lal, F. Navarro, C. A. Maher, L. E. Maliszewski, N. Yan, E. O'Day, D. Chowdhury,
1017 D. M. Dykxhoorn, P. Tsai, O. Hofmann, K. G. Becker, M. Gorospe, W. Hide, J.
1018 Lieberman, miR-24 Inhibits Cell Proliferation by Targeting E2F2, MYC, and Other
1019 Cell-Cycle Genes via Binding to "Seedless" 3′UTR MicroRNA Recognition Elements.
1020 *Mol. Cell*. **35**, 610–625 (2009).
1021 32. M. Sachdeva, S. Zhu, F. Wu, H. Wu, V. Walia, S. Kumar, R. Elble, K. Watabe, Y. Y.
1022 Mo, p53 represses c-Myc through induction of the tumor suppressor miR-145. *Proc.*

1023 *Natl. Acad. Sci. U. S. A.* **106**, 3207–3212 (2009).
1024 33. N. M. Yeilding, M. T. Rehman, W. M. Lee, Identification of sequences in c-myc mRNA
1025 that regulate its steady-state levels. *Mol. Cell. Biol.* **16**, 3511–3522 (1996).
1026 34. D. Caput, B. Beutler, K. Hartog, R. Thayer, S. Brown-Shimer, A. Cerami, Identification
1027 of a common nucleotide sequence in the 3'-untranslated region of mRNA molecules
1028 specifying inflammatory mediators. *Proc. Natl. Acad. Sci. U. S. A.* (1986),
1029 doi:10.1073/pnas.83.6.1670.
1030 35. K. Kataoka, Y. Shiraishi, Y. Takeda, S. Sakata, M. Matsumoto, S. Nagano, T. Maeda,
1031 Y. Nagata, A. Kitanaka, S. Mizuno, H. Tanaka, K. Chiba, S. Ito, Y. Watatani, N.
1032 Kakiuchi, H. Suzuki, T. Yoshizato, K. Yoshida, M. Sanada, H. Itonaga, Y. Imaizumi, Y.
1033 Totoki, W. Munakata, H. Nakamura, N. Hama, K. Shide, Y. Kubuki, T. Hidaka, T.
1034 Kameda, K. Masuda, N. Minato, K. Kashiwase, K. Izutsu, A. Takaori-Kondo, Y.
1035 Miyazaki, S. Takahashi, T. Shibata, H. Kawamoto, Y. Akatsuka, K. Shimoda, K.
1036 Takeuchi, T. Seya, S. Miyano, S. Ogawa, Aberrant PD-L1 expression through 3′-UTR
1037 disruption in multiple cancers. *Nature*. **534**, 402–406 (2016).
1038 36. M. W. Hentze, A. Castello, T. Schwarzl, T. Preiss, A brave new world of RNA-binding
1039 proteins. *Nat. Rev. Mol. Cell Biol.* **19**, 327–341 (2018).
1040 37. C. Ko, W. Wang, C. Li, Y. Jeng, Y. Chu, H. Wang, J. T. Tseng, J. Wang, IL-18-
1041 induced interaction between IMP3 and HuR contributes to COX-2 mRNA stabilization
1042 in acute myeloid leukemia. *J. Leukoc. Biol.* **99**, 131–141 (2016).
1043 38. A. Vujovic, L. de Rooij, A. Keyvani Chahi, H. T. Chen, B. A. Yee, S. K. Loganathan, L.
1044 Liu, D. C. H. Chan, A. Tajik, E. Tsao, S. Moreira, P. Joshi, J. Xu, N. Wong, Z. Balde,
1045 S. Jahangiri, S. Zandi, S. Aigner, J. E. Dick, M. D. Minden, D. Schramek, G. W. Yeo,
1046 K. J. Hope, In vivo screening unveils pervasive RNA-binding protein dependencies in
1047 leukemic stem cells and identifies ELAVL1 as a therapeutic target. *Blood Cancer*
1048 *Discov.* (2023), doi:10.1158/2643-3230.BCD-22-0086.
1049 39. K. Rothamel, ELAVL1 Exclusively Couples mRNA Stability with the 3'UTRs of
1050 Interferon Stimulated Genes. *bioRxiv* (2020).
1051 40. R. Kuuselo, K. Savinainen, S. Sandström, R. Autio, A. Kallioniemi, MED29, a
1052 component of the mediator complex, possesses both oncogenic and tumor
1053 suppressive characteristics in pancreatic cancer. *Int. J. Cancer*. **129**, 2553–2565
1054 (2011).
1055 41. T. C. Lin, C. Y. Su, P. Y. Wu, T. C. Lai, W. A. Pan, Y. H. Jan, Y. C. Chang, C. T. Yeh,
1056 C. L. Chen, L. P. Ger, H. T. Chang, C. J. Yang, M. S. Huang, Y. P. Liu, Y. F. Lin, J. Y.
1057 J. Shyy, M. D. Tsai, M. Hsiao, The nucleolar protein NIFK promotes cancer
1058 progression via ck1α/β-catenin in metastasis and ki-67-dependent cell proliferation.
1059 *Elife*. **5**, 1–21 (2016).
1060 42. F. F. Blanco, R. Preet, A. Aguado, V. Vishwakarma, L. E. Stevens, A. Vyas, S.
1061 Padhye, L. Xu, S. J. Weir, S. Anant, N. Meisner-Kober, J. R. Brody, D. A. Dixon,
1062 Impact of HuR inhibition by the small molecule MS-444 on colorectal cancer cell
1063 tumorigenesis. *Oncotarget* (2016), doi:10.18632/oncotarget.12189.
1064 43. D. Hnisz, B. J. Abraham, T. I. Lee, A. Lau, V. Saint-André, A. A. Sigova, H. A. Hoke,
1065 R. A. Young, Super-enhancers in the control of cell identity and disease. *Cell* (2013),
1066 doi:10.1016/j.cell.2013.09.053.
1067 44. B. E. Gryder, L. Wu, G. M. Woldemichael, S. Pomella, T. R. Quinn, P. M. C. Park, A.
1068 Cleveland, B. Z. Stanton, Y. Song, R. Rota, O. Wiest, M. E. Yohe, J. F. Shern, J. Qi,
1069 J. Khan, Chemical genomics reveals histone deacetylases are required for core
1070 regulatory transcription. *Nat. Commun.* **10**, 1–12 (2019).
1071 45. B. Schwanhüusser, D. Busse, N. Li, G. Dittmar, J. Schuchhardt, J. Wolf, W. Chen, M.
1072 Selbach, Global quantification of mammalian gene expression control. *Nature*. **473**,
1073 337–342 (2011).
1074 46. C. Mayr, D. P. Bartel, Widespread Shortening of 3′UTRs by Alternative Cleavage and
1075 Polyadenylation Activates Oncogenes in Cancer Cells. *Cell*. **138**, 673–684 (2009).
1076 47. C. Vicente, R. Stirparo, S. Demeyer, C. E. De Bock, O. Gielen, M. Atkins, J. Yan, G.
1077 Halder, B. A. Hassan, J. Cools, The CCR4-NOT complex is a tumor suppressor in
1078 Drosophila melanogaster eye cancer models. *J. Hematol. Oncol.* (2018),
1079 doi:10.1186/s13045-018-0650-0.
1080 48. S. Weißbach, C. Langer, B. Puppe, T. Nedeva, E. Bach, M. Kull, R. Bargou, H.
1081 Einsele, A. Rosenwald, S. Knop, E. Leich, The molecular spectrum and clinical impact

1082 of DIS3 mutations in multiple myeloma. *Br. J. Haematol.* (2015),
1083 doi:10.1111/bjh.13256.
1084 49. C. Desterke, A. Bennaceur-Griscelli, A. G. Turhan, DIS3 Mutation in RUNX1-Mutated
1085 AML1 Confers a Highly Dismal Prognosis in AML By Repressing Sister Chromatid
1086 Cohesion. *Blood* (2019), doi:10.1182/blood-2019-123352.
1087 50. D. F. Aghib, J. M. Bishop, A 3' truncation of myc caused by chromosomal
1088 translocation in a human T-cell leukemia is tumorigenic when tested in established rat
1089 fibroblasts. *Oncogene*. **6**, 2371–5 (1991).
1090 51. D. F. Aghib, J. M. Bishop, S. Ottolenghi, A. Guerrasio, A. Serra, G. Saglio, A 3'
1091 truncation of MYC caused by chromosomal translocation in a human T-cell leukemia
1092 increases mRNA stability. *Oncogene*. **5**, 707–11 (1990).
1093 52. Z. Xia, L. A. Donehower, T. A. Cooper, J. R. Neilson, D. A. Wheeler, E. J. Wagner, W.
1094 Li, Dynamic analyses of alternative polyadenylation from RNA-seq reveal a 3'2-UTR
1095 landscape across seven tumour types. *Nat. Commun.* **5** (2014),
1096 doi:10.1038/ncomms6274.
1097 53. F. Yuan, W. Hankey, E. J. Wagner, W. Li, Q. Wang, Alternative polyadenylation of
1098 mRNA and its role in cancer. *Genes Dis.* **8**, 61–72 (2021).
1099 54. S. Kammler, S. Lykke-Andersen, T. H. Jensen, The RNA exosome component hRrp6
1100 is a target for 5-fluorouracil in human cells. *Mol. Cancer Res.* **6**, 990–995 (2008).
1101 55. R. A. Silverstein, E. G. De Valdivia, N. Visa, The incorporation of 5-fluorouracil into
1102 RNA affects the ribonucleolytic activity of the exosome subunit Rrp6. *Mol. Cancer*
1103 *Res.* **9**, 332–340 (2011).
1104 56. T. Yamauchi, T. Masuda, M. C. Canver, M. Seiler, Y. Semba, M. Shboul, M. Al-
1105 Raqad, M. Maeda, V. A. C. Schoonenberg, M. A. Cole, C. Macias-Trevino, Y.
1106 Ishikawa, Q. Yao, M. Nakano, F. Arai, S. H. Orkin, B. Reversade, S. Buonamici, L.
1107 Pinello, K. Akashi, D. E. Bauer, T. Maeda, Genome-wide CRISPR-Cas9 Screen
1108 Identifies Leukemia-Specific Dependence on a Pre-mRNA Metabolic Pathway
1109 Regulated by DCPS. *Cancer Cell*. **33**, 386-400.e5 (2018).
1110 57. D. Hanahan, R. A. Weinberg, Hallmarks of cancer: The next generation. *Cell*. **144**,
1111 646–674 (2011).
1112 58. M. Rashkovan, A. Ferrando, Metabolic dependencies and vulnerabilities in leukemia.
1113 *Genes Dev.* **33**, 1460–1474 (2019).
1114 59. K. Rothamel, S. Arcos, B. Kim, C. Reasoner, S. Lisy, N. Mukherjee, K. Rothamel, S.
1115 Arcos, B. Kim, C. Reasoner, S. Lisy, N. Mukherjee, ELAVL1 primarily couples mRNA
1116 stability with the 3 0 UTRs of interferon-stimulated genes ll ll ELAVL1 primarily
1117 couples mRNA stability with the 3 0 UTRs of interferon-stimulated genes. *Cell Rep.*
1118 **35**, 109178 (2021).
1119 60. S. Heinzel, T. Binh Giang, A. Kan, J. M. Marchingo, B. K. Lye, L. M. Corcoran, P. D.
1120 Hodgkin, A Myc-dependent division timer complements a cell-death timer to regulate
1121 T cell and B cell responses. *Nat. Immunol.* (2017), doi:10.1038/ni.3598.
1122 61. C. Ye, D. J. Ho, M. Neri, C. Yang, T. Kulkarni, R. Randhawa, M. Henault, N. Mostacci,
1123 P. Farmer, S. Renner, R. Ihry, L. Mansur, C. G. Keller, G. Mcallister, M. Hild, J.
1124 Jenkins, A. Kaykas, DRUG-seq for miniaturized high-throughput transcriptome
1125 profiling in drug discovery. *Nat. Commun.*, 1–9 (2018).
1126 62. A. Subramanian, P. Tamayo, V. K. Mootha, S. Mukherjee, B. L. Ebert, M. A. Gillette,
1127 A. Paulovich, S. L. Pomeroy, T. R. Golub, E. S. Lander, J. P. Mesirov, Gene set
1128 enrichment analysis: A knowledge-based approach for interpreting genome-wide
1129 expression profiles. *Proc. Natl. Acad. Sci. U. S. A.* (2005),
1130 doi:10.1073/pnas.0506580102.
1131 63. J. Chen, H. Xu, B. J. Aronow, A. G. Jegga, Improved human disease candidate gene
1132 prioritization using mouse phenotype. *BMC Bioinformatics*. **8**, 1–13 (2007).
1133 64. J. Chen, E. E. Bardes, B. J. Aronow, A. G. Jegga, ToppGene Suite for gene list
1134 enrichment analysis and candidate gene prioritization. *Nucleic Acids Res.* **37**, 305–
1135 311 (2009).
1136 65. J. Chen, B. J. Aronow, A. G. Jegga, Disease candidate gene identification and
1137 prioritization using protein interaction networks. *BMC Bioinformatics*. **10**, 1–14 (2009).
1138 66. Z. Wang, J. Hu, E. W. Johnson, J. D. Campbell, Scruff: An R/Bioconductor package
1139 for preprocessing single-cell RNA-sequencing data. *bioRxiv*, 1–9 (2019).
1140 67. T. Stuart, A. Butler, P. Hoffman, C. Hafemeister, E. Papalexi, W. M. Mauck, Y. Hao,

1141 M. Stoeckius, P. Smibert, R. Satija, Comprehensive Integration of Single-Cell Data.
1142 *Cell* (2019), doi:10.1016/j.cell.2019.05.031.
1143 68. H. A. Hoke, C. Y. Lin, A. Lau, D. A. Orlando, C. R. Vakoc, J. E. Bradner, T. I. Lee, R.
1144 A. Young, Selective Inhibition of Tumor Oncogenes by Disruption of Super-Enhancers
1145 (2013), doi:10.1016/j.cell.2013.03.036.
1146 69. S. J. Vervoort, S. A. Welsh, J. R. Devlin, E. Barbieri, D. A. Knight, S. Offley, S.
1147 Bjelosevic, M. Costacurta, I. Todorovski, C. J. Kearney, J. J. Sandow, Z. Fan, B.
1148 Blyth, V. McLeod, J. H. A. Vissers, K. Pavic, B. P. Martin, G. Gregory, E.
1149 Demosthenous, M. Zethoven, I. Y. Kong, E. D. Hawkins, S. J. Hogg, M. J. Kelly, A.
1150 Newbold, K. J. Simpson, O. Kauko, K. F. Harvey, M. Ohlmeyer, J. Westermarck, N.
1151 Gray, A. Gardini, R. W. Johnstone, The PP2A-Integrator-CDK9 axis fine-tunes
1152 transcription and can be targeted therapeutically in cancer. *Cell*. **184**, 3143-3162.e32
1153 (2021).
1154 70. B. Sundararaman, L. Zhan, S. M. Blue, R. Stanton, K. Elkins, S. Olson, X. Wei, E. L.
1155 Van Nostrand, G. A. Pratt, S. C. Huelga, B. M. Smalec, X. Wang, E. L. Hong, J. M.
1156 Davidson, E. Lécuyer, B. R. Graveley, G. W. Yeo, Resources for the Comprehensive
1157 Discovery of Functional RNA Elements. *Mol. Cell*. **61**, 903–913 (2016).
1158 71. B. Li, C. N. Dewey, RSEM: accurate transcript quantification from RNA-Seq data with
1159 or without a reference genome. *BMC Bioinformatics*. **12**, 323 (2011).
1160 72. S. J. Vervoort, S. A. Welsh, J. R. Devlin, N. Gray, A. Gardini, R. W. Johnstone, The
1161 PP2A-Integrator-CDK9 axis fine-tunes transcription and can be targeted
1162 therapeutically in cancer. *Cell*, 1–20 (2021).
1163

Figures

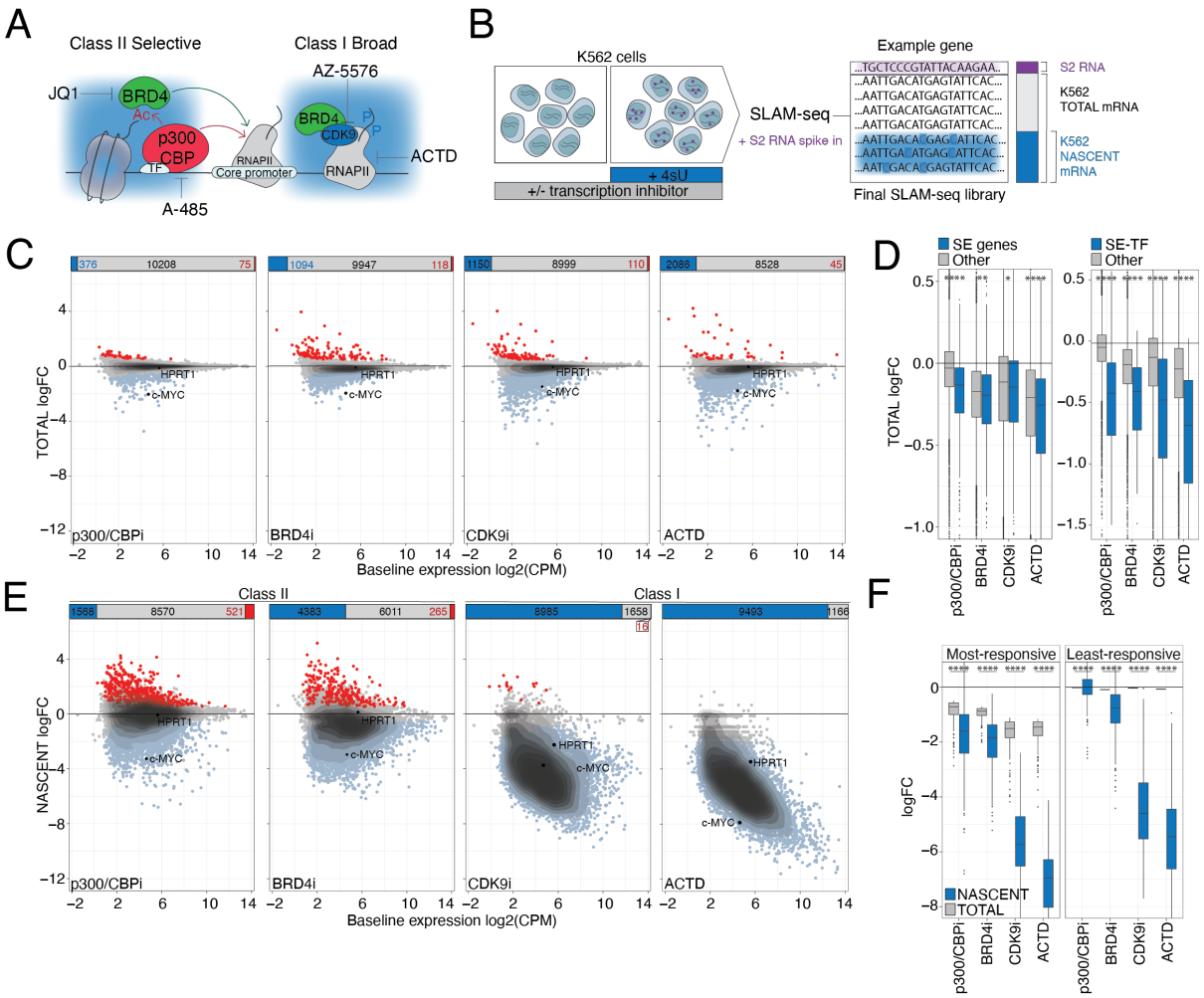

Figure 1. A defined subset of genes determines the therapeutic response to transcription inhibition. **(A)** Simplified schematic of transcription inhibition by A-485 (p300/CBPi), JQ1 (BRD4i), AZ-5576 (CDK9i) and Actinomycin-D (ACTD). **(B)** Schematic of SLAM-seq experimental procedure. Nascent reads are defined as RNA containing at least two thymine-to-cytosine (T>C) conversions and total reads are defined as the sum of unconverted and converted RNA. Schneider 2 (S2) RNA was spiked-in as an external reference control. **(C)** Scatterplot of baseline total mRNA expression versus change in spike-in normalized total gene expression upon two hours of transcription inhibition. Significantly up- or down-regulated genes highlighted in red and blue, respectively. Sum of significantly differentially altered events indicated in bar chart above. **(D)** Change in spike-in normalized total expression of **(left)** genes regulated by super-enhancers (SEs) and **(right)** core-regulatory transcription factors (SE-TF). Remaining genes indicated in grey. **(E)** Scatterplot of baseline nascent mRNA expression versus change in spike-in normalized total gene expression upon two hours of transcription inhibition. Significantly up- or down-regulated genes highlighted in red and blue, respectively. Sum of significantly differentially altered events indicated in bar chart above. **(F)** Change in spike-in normalized total and nascent expression of **(left)** most- and **(right)** least-responsive genes.

p300/CBP: p300/cAMP-response element binding protein (CBP). BRD4: Bromodomain-Containing Protein 4. CDK9: Cyclin Dependent Kinase 9. RNAPII: RNA Polymerase II. TF: Transcription factor. Ac: Acetyl group. P: Phosphate group. 4sU: 4-thiouridine. H: Hour. 3'UTR: 3' Untranslated Region. LogFC: log2 fold change relative to DMSO. Baseline expression: spike-in normalized total log2 CPM in DMSO-treated conditions. CPM: Counts Per Million. Significantly up-regulated: P Value < 0.05 & logFC > 0.5. Significantly down-regulated: P Value < 0.05 & logFC < -0.5. P Value < 0.0001 using an unpaired Wilcoxon test. Most-responsive: top 200 most significantly down-regulated genes

1190 (logFC < -0.5 and P Value < 0.05) using spike-in normalized total reads. Least-responsive: 200
1191 unaltered (-0.25 < logFC < 0.25 and P Value > 0.05) genes using spike-in normalized total reads.
1192 AUC: Area Under the Curve.

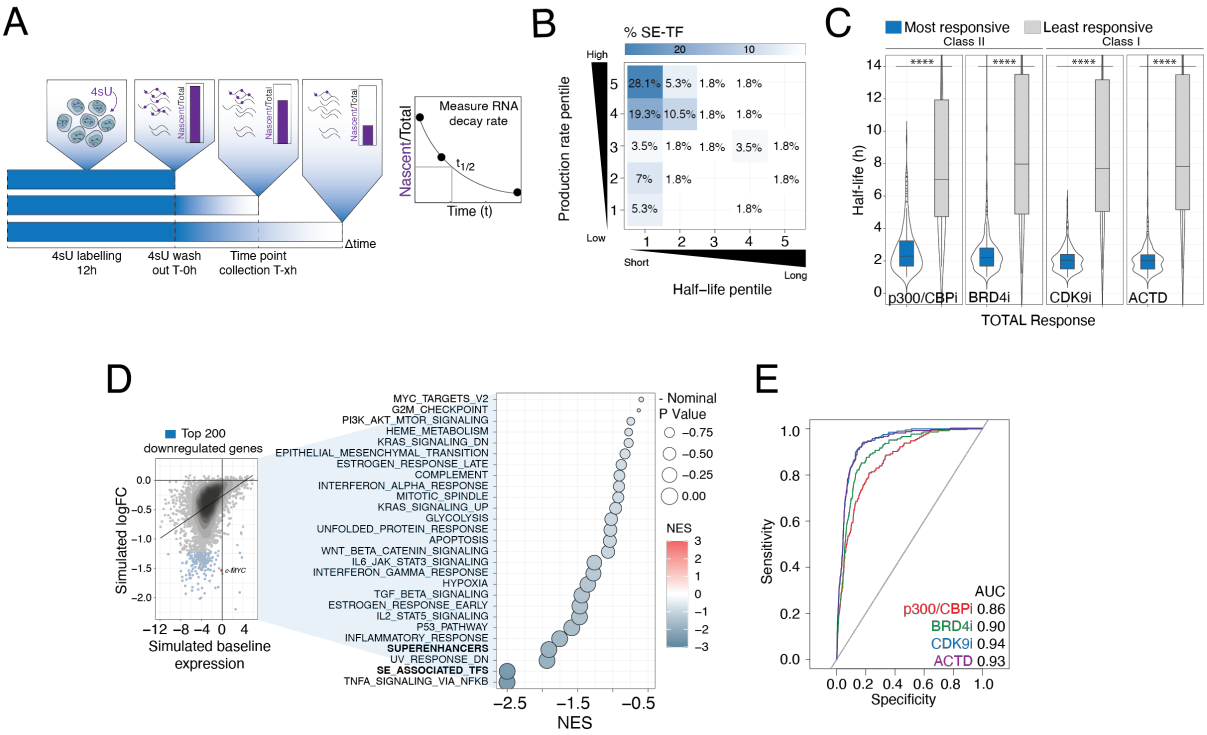

Figure 2. Gene intrinsic RNA decay properties shape the therapeutic response to transcriptional inhibitors.

(A) Schematic of 4-thiouridine (4sU) pulse labelling and chase. T > C conversion rates were calculated for each time point, normalized to 0-h and fit with exponential decay functions derive half-life ($t_{1/2}$). **(B)** Heatmap of percentage of CR TFs present within each mRNA decay and production pentiles from Fig. S4. F. **(C)** Boxplot of mRNA half-lives of genes most- and least-responsive to treatments indicated. **(D) (Right)** Simulation of total mRNA levels with complete transcription shutdown after two hours and **(left)** associated GSEA analysis of hallmark, SE and SE-associated TF gene sets using ranked z-scored logFC values. Signatures with Normalized Enrichment Scores (NES) < 0 shown. **(E)** Receiver Operator Characteristic (ROC) analysis of total logFC with treatments indicated and simulated total logFC after complete transcription shutdown for 2 hours. logFC values were binarized according to whether genes were most-responsive to treatments indicated.

AUC: Area Under the Curve. Most-responsive: top 200 most significantly down-regulated genes (logFC < -0.5 and P Value < 0.05) using spike-in normalized reads. Least-responsive: 200 unaltered (-0.25 < logFC < 0.25 and P Value > 0.05) genes using spike-in normalized reads.

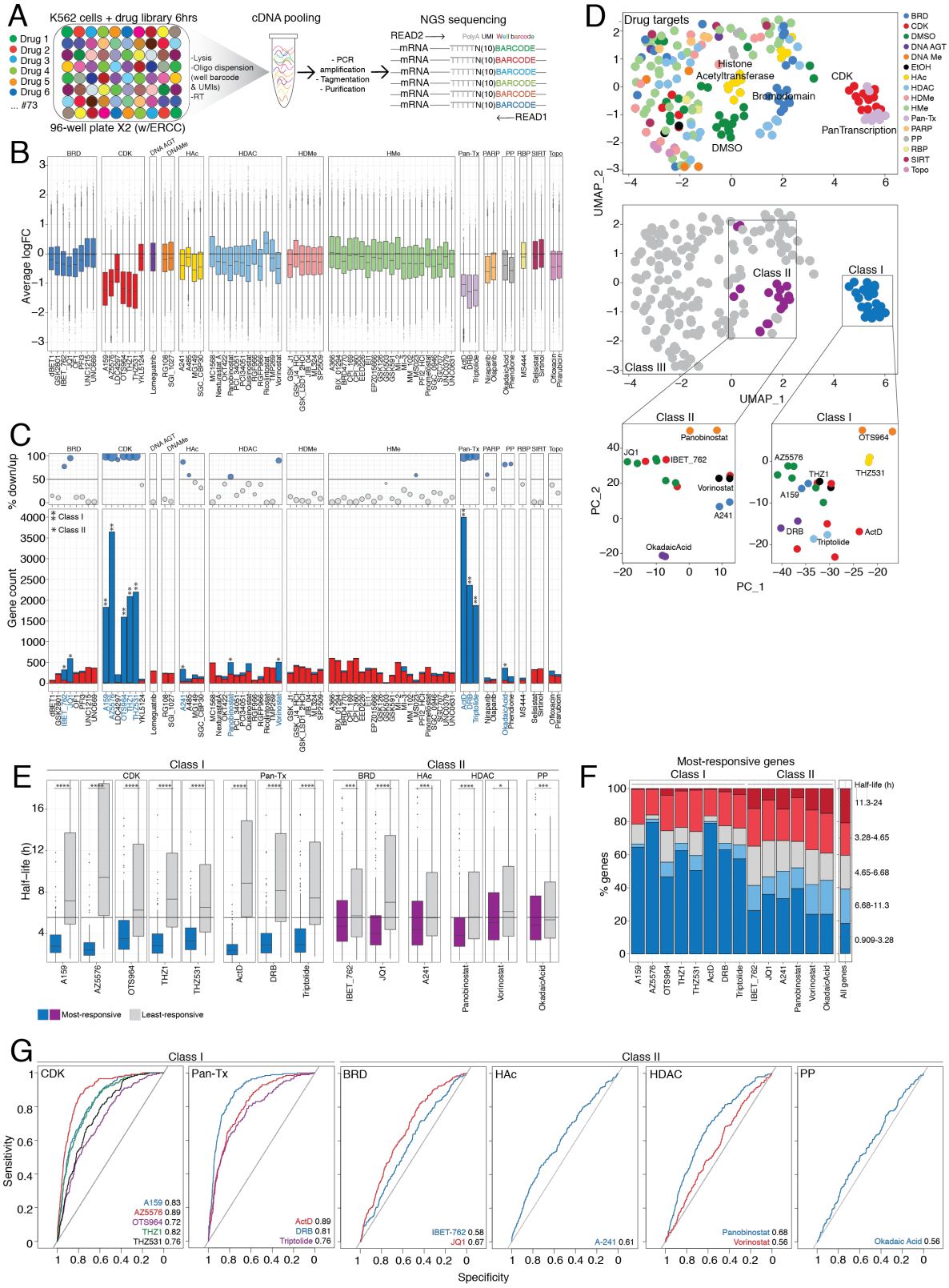

Figure 3. Gene intrinsic RNA decay properties shape the therapeutic response to several epigenetic and transcriptional inhibitors as defined by MAC-seq.

(A) Schematic of MAC-seq experimental procedure. **(B)** Box plot of change in gene expression relative to DMSO/EtOH controls with inhibitors indicated. Inhibitors are grouped according to drug protein target family. **(C)** (***Top***) Percentage ratio or (***bottom***) absolute number of significantly up- and down-regulated genes. Inhibitors able to significantly down-regulate > 1000 genes are termed 'Class I' and by **. Inhibitors able to significantly down-regulate > 200 genes are termed 'Class II'

and indicated by *. Remaining compounds as designated as class III. **(D)** Uniform Manifold Approximation and Projection (UMAP) of treatment conditions with **(*top*)** drug protein target family **(*middle*)** or pre-defined classes highlighted. **(*Bottom*)** PCA plot of drug classes **(right)** II and **(left)** I with drug names shown. **(E)** Boxplot of mRNA half-life of most- and least-responsive genes to class I and II inhibitors. **(F)** Bar chart representation of mRNA half-life pentiles in genes most-responsive to class I and II inhibitors. **(G)** Receiver Operator Characteristic (ROC) analysis of logFC with class I and II inhibitors and simulated total logFC after complete transcription shutdown for 6 hours. logFC values were binarized according to whether genes were most-responsive to treatments indicated.
UMI: Unique Molecular Identifier. logFC: log2 fold change. BRD: Bromodomain. CDK: Cyclin Dependant Kinase. DNA AGT: DNA alkyl-transferase. DNAMe: DNA methyl-transferase. HAc: Histone acetylase. HDAC: Histone deacetylase. HDMe: Histone demethylase. HMe: Histone methyl-transferase. Pan-Tx: Pan-transcription. PP: Protein Phosphotase. RBP: RNA Binding Protein. SIRT: Sirtuin. Topo: Topoisomerase. Significantly up-regulated: P-Value < 0.05 and average logFC > 0.5. Significantly down-regulated: P-Value < 0.05 and average logFC < -0.5. logFC: log2 fold change relative to DMSO/EtOH. AUC: Area Under the Curve. Most-responsive: top 200 most significantly down-regulated genes (logFC < -0.5 and P Value < 0.05) using spike-in normalized reads. Least-responsive: 200 unaltered (-0.25 < logFC < 0.25 and P Value > 0.05) genes using spike-in normalized reads.

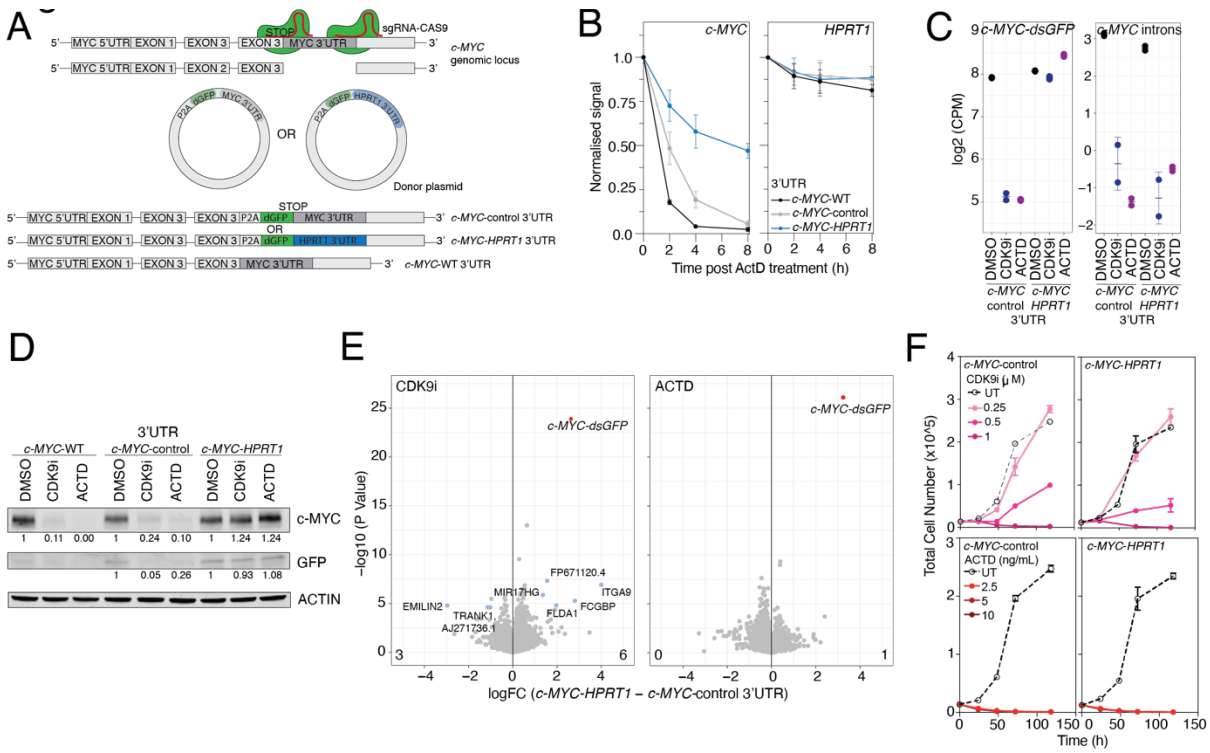

Figure 4. Increased *c-MYC* RNA stability does not rescue biological and transcriptional effects of transcriptional inhibitors**.**

(A) Schematic of CRISPR/Cas9 -homology directed repair (HDR) used to endogenously swap the *c-MYC* 3' untranslated region (3'UTR) for the *HPRT1* 3'UTR in the K562 cell line. **(B)** Normalized expression of **(left)** *c-MYC* and **(right)** *HPRT1* transcripts following the addition of ACTD at indicated time points as measured by quantitative real time PCR (qRT-PCR). Values are mean with error bars representing standard deviation (sd) of three biological replicates from three separate single cell clones. **(C) (Left)** Total gene expression of reads mapping across *c-MYC* and *dsGFP* sequences with indicated treatments and cell lines after 6 hours. **(Right)** *c-MYC* intron expression with indicated treatments and cell lines after 6 hours. **(D)** Western blot of **(top)** c-MYC, **(middle)** GFP and **(bottom)** ACTIN protein with indicated treatments and cell lines after six hours. Values indicated are protein levels normalized to ACTIN and DMSO controls. **(E)** Scatter plot of significance and difference in total gene expression with **(left)** CDK9i and **(right)** ACTD treatment between *c-MYC*-control and -*HPRT1* 3'UTR cell lines. **(F)** Total cell number over time of indicated cell lines treated with increasing concentrations of **(top)** CDK9i and **(bottom)** ACTD.

logFC: log2 fold change.

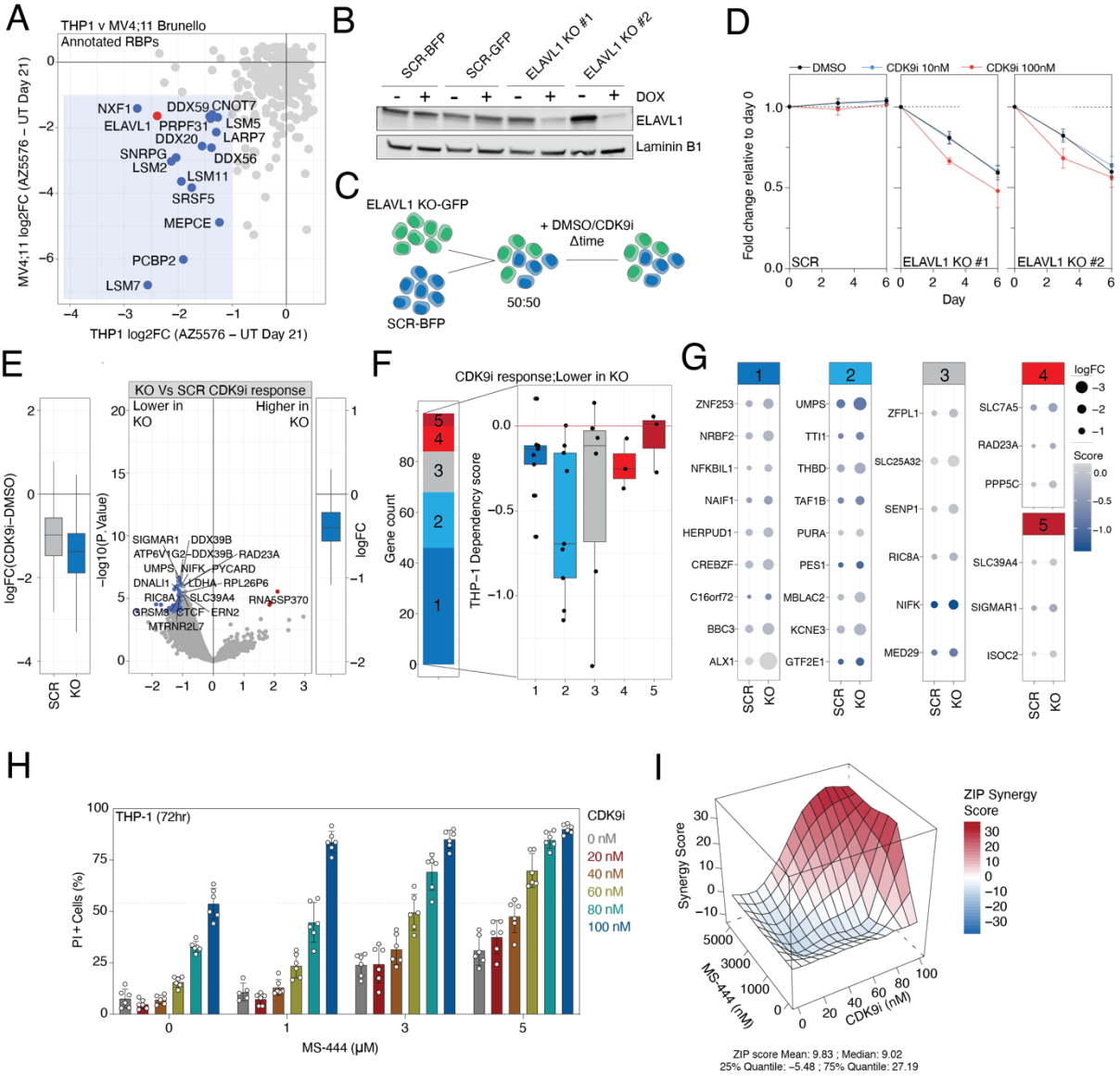

Figure 5. Dual targeting of CDK9 and ELAVL1 is synergistic in AML.
(A) Scatter plot of change in sgRNA read counts in CDK9i compared to untreated (UT) CRISPR-Cas9 genome-wide screening groups after 21 days of passaging in THP-1 and MV4;11 AML cell lines. Annotated RBPs that are down-regulated (logFC < -1) in both THP-1 and MV;11 cell lines indicated in blue and red (ELAVL1). Data is obtained from (*72*). **(B)** Western blot of **(top)** ELAVL1 and **(bottom)** Laminin B1 protein with indicated treatments and THP-1 cell lines after four days. **(C)** Simplified schematic of competition assay experimental design. THP-1 cells expressing Cas9 and non-targeting control sgRNA (SCR) and sgRNAs targeting ELAVL1 (ELAVL1 knockout) are mixed in a 1:1 ratio and passaged in the presence of DMSO or CDK9i. **(D)** Fold change relative to day 0 of THP1 ELAVL1 knockout cells in competition with SCR cells as described in (C) at time points and treatments indicated. **(E) (Left)** Boxplot of spike-in normalized total mRNA reads with CDK9i relative to DMSO in THP-1 SCR and ELAVL1 KO cells. **(Right)** Scatter plot of significance and difference in spike-in normalized total gene expression of CDK9i response in ELAVL1 knockout relative to SCR cells. Significantly down- and up-regulated genes are highlighted in blue and red, respectively. **(F) (Left)** Stacked bar chart of previously determined transcript half-life pentiles in THP-1 cells across mRNAs sensitized to CDK9i upon ELAVL1 knockout (lower in KO; logFC < -1 and adjusted P Value < 0.01) and **(Right)** associated boxplot and **(G)** dot plot of THP-1 gene dependency scores from the Broad Institute Cancer Dependancy Map. LogFC values in each cell line are indicated. **(H)** Bar plot of THP-1 cell death (propidium iodide (PI) positive) in response to CDK9i and MS-444 at concentrations indicated following 72 hours. **(I)** ZIP synergy scores derived from (H). Representative of first replicate.

logFC: log2 fold change. SCR: non-targeting sgRNA control. KO: knockout. Significantly down-regulated: logFC < -1 and adjusted P Value < 0.01. Significantly up-regulated: logFC > 1 and adjusted P Value < 0.01.

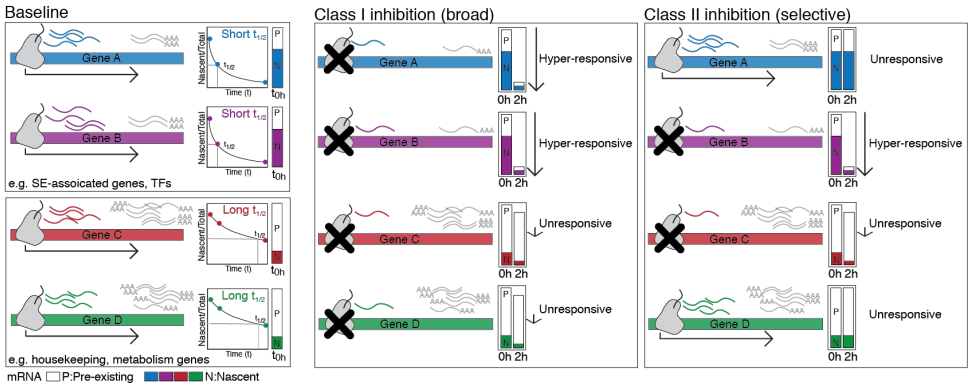

Figure 6. Simplified schematic of transcriptional responses of genes with short and long RNA half-lives with class I (selective) and class II (broad) inhibitors.